Magnetic topology of Active Regions and Coronal Holes: Implications for Coronal Outflows and the Solar Wind

L. van Driel-Gesztelyi[1, 2, 3] • J. L. Culhane[1,4] • D. Baker[1] • P. Démoulin[2] • C.H. Mandrini[5,6] • M.L. DeRosa[7] • A. P. Rouillard[8,9] • A. Opitz[8,9] • G. Stenborg[10] • A. Vourlidas[11] • D. H. Brooks[10]

[1]University College London, Mullard Space Science Laboratory, Dorking, UK,
[2]Observatoire de Paris, LESIA, CNRS, UPMC Univ. Paris 06, Univ. Paris-Diderot, Meudon, France, email: Lidia.vanDriel@obspm.fr
[3]Konkoly Observatory, Hungarian Academy of Sciences, Budapest, Hungary,
[4]International Space Science Institute, Bern, Switzerland,
[5]Instituto de Astronomía y Física del Espacio, CONICET-UBA, CC. 67, Suc. 28, 1428 Buenos Aires, Argentina,
[6]Facultad de Ciencias Exactas y Naturales, FCEN-UBA, Buenos Aires, Argentina,
[7] Lockheed Martin Solar and Astrophysics Laboratory, Palo Alto, CA 94304, USA,
[8] Institut de Recherche en Astrophysique et Planétologie, Université de Toulouse (UPS), France
[9] Centre National de la Recherche Scientifique, UMR 5277, Toulouse, France
[10]College of Science, George Mason University, Fairfax, VA 22030, USA,
[11]Space Science Division, Naval Research Laboratory, Washington, DC 20375, USA

Abstract

During 2 – 18 January 2008 a pair of low-latitude opposite-polarity coronal holes (CHs) were observed on the Sun with two active regions (ARs) and the heliospheric plasma sheet located between them. We use the *Hinode/EUV Imaging Spectrometer* (EIS) to locate AR-related outflows and measure their velocities. *Solar-Terrestrial Relations Observatory* (STEREO) imaging is also employed as are the *Advanced Composition Explorer* (ACE) *in-situ* observations, to assess the resulting impacts on the interplanetary solar wind (SW) properties. Magnetic field extrapolations of the two ARs confirm that AR plasma outflows observed with EIS are co-spatial with quasi-separatrix layer locations, including the separatrix of a null point. Global potential field source-surface modeling indicates that field lines in the vicinity of the null point extend up to the source surface, enabling a part of the EIS plasma upflows access to the SW. We find that similar upflow properties are also observed within closed-field regions that do not reach the source surface. We conclude that some of plasma upflows observed with EIS remain confined along closed coronal loops, but that a fraction of the plasma may be released in the slow SW. This suggests that ARs bordering coronal holes can contribute to the slow SW. Analyzing the *in-situ* data, we propose that the type of slow SW present depends on whether the AR is fully or partially enclosed by an overlying streamer.

Keywords: Active regions, magnetic field, magnetic extrapolations, solar wind

Running Title: Magnetic Topology, Coronal Outflows, and the Solar Wind
Running Author: L. van Driel-Gesztelyi *et al.*

1. Introduction

Persistent and intermittent outflows from active regions (ARs) have been observed with the *Transition Region and Coronal Explorer* (TRACE) Extreme Ultraviolet (EUV) telescope with velocities in the range 5 – 20 km s^{-1} (Winebarger, DeLuca, and Golub, 2001). In the absence of any periodicities, the authors ascribed these flows as resulting from discrete reconnection events. More recently Sakao *et al.* (2007) using the *Hinode*/*X-ray Telescope* (XRT: Golub *et al.,* 2007) have identified continuous plasma outflows along extended large AR loops. They estimated that a contribution of ≤ 25% to the slow SW is possible. The same target region has been observed by Harra et al. (2008) using the *Hinode/EUV Imaging Spectrometer* (EIS: Culhane *et al.*, 2007) who found line of sight velocities of 20 km s^{-1} to 50 km s^{-1} but, by comparison with a magnetic-field extrapolation for the AR, estimated that the true velocities could reach over 100 km s^{-1}.

Following this work, several further observations of AR-associated outflows have been reported. Such flows are generally observed at AR peripheries and not in the AR cores. Doschek *et al*. (2007, 2008) and Del Zanna (2008) found that the flows are variable, are from areas of weak Fe XII line intensity, are usually associated with a single magnetic polarity region, and can last for several days. They also suggested that the significant line broadening, observed to correlate with outflow velocity, along with the appearance of blue wing asymmetries (see also Hara *et al.,* 2008; Bryans, Young, and Doschek, 2010) could indicate the presence of multiple flow sites at different speeds. Warren *et al.* (2011) observed upflows up to T_e = 2.5 MK (Fe XV) but with no blue-shifted emission at lower temperatures ($T_e \approx$ 0.63 MK in Si VII) where down-flowing plasma was detected along coronal fan-like loop structures, which appeared to have a different morphology to that of the outflows. They concluded that the peripheral outflows are probably not associated with a fan-loop population, which connects to close-by quiet-Sun polarities, as the latter represent mainly closed magnetic field lines. Based on temporal variability observations, Ugarte-Urra and Warren (2011) support this conclusion.

From TRACE observations, Schrijver *et al.* (1999) established the existence of cooler loops ($T_e \approx$ 1 MK) at AR peripheries that are long fan-like structures extending away from the parent AR. These fan-loops can connect with other ARs, to remote parts of the parent AR and even to the quiet Sun. Spectroscopic observations have confirmed their low temperature ($T_e \leq$ 1 MK; Del Zanna, 2003; Young *et al.,* 2007) along with the presence of persistent redshifts indicating downflows (Winebarger *et al.,* 2002; Marsch, Wiegelmann, and Xia, 2004; Del Zanna, 2008; Warren *et al.,* 2011). Following the suggestion that upflows (50 – 150 km s^{-1}) from the recently identified Type II spicules, observed from all parts of the chromosphere may play a significant role in coronal heating (De Pontieu *et al.,* 2007, 2009) more recent work by Tian, McIntosh, and De Pontieu (2011), based on EIS raster scanning and *Atmospheric Imaging Assembly* (AIA) observations (Lemen *et al.,* 2012), suggests that at least a part of the AR-associated outflows can be identified with periodic disturbances seen in the fan-loop plasma. Discussion of the driving mechanisms for the spicule-related flows is beyond the scope of this article.

After the discovery of AR outflows, several possible driving mechanisms were suggested. These included magnetic-field funnels causing coronal plasma circulation (Marsch *et al.,* 2008), impulsive heating at loop footpoints (Hara *et al.,* 2008),

evaporation upflows due to flux emergence (Del Zanna, 2008), expansion of large-scale reconnected loops (Harra *et al.,* 2008), reconnection at quasi-separatrix layers (QSLs) involving AR structures and surrounding field (Baker *et al.,* 2009), plasma compression due to AR expansion (Murray *et al.,* 2010), new flux emergence within a pre-existing AR (Harra et al., 2012), and interchange reconnection at a high coronal null-point with a resulting pressure gradient driving a rarefaction wave (Del Zanna *et al.*, 2011; Bradshaw, Aulanier, and Del Zanna, 2011).

It is thought that interchange reconnection takes place between open and closed field lines that exchange footpoints between them. For example, if an emerging closed field interacts with pre-existing open fields, coronal jets can result (Shibata *et al.,* 1992) producing fast outflows. However, for the configuration that we will analyze below, the observed outflows emerge from a unipolar field region located at an AR/coronal hole (CH) boundary. The peripheral AR outflows observed by the EIS instrument frequently occur at sites where magnetic-field lines display strong gradients in connectivity over unipolar regions. These sites are thought to be the locations of QSLs (Démoulin *et al.,* 1996) or, in the limit of infinitely large gradients, separatrices. QSLs are defined by the global properties of the magnetic field and therefore evolve slowly. They are preferential locations for current-sheet formation and magnetic reconnection can still occur through component reconnection provided that there is a significant angle between the field lines involved (Baker *et al.,* 2009).

Whether or not these flows are generated on closed or open magnetic field structures is of great importance in relation to their possible contribution to the slow solar wind. Although it is generally agreed that the fast SW ($v \geq 600$ km s^{-1}) originates in coronal holes, the source of the slow wind ($v \leq 450$ km s^{-1}) is still a matter of debate. While the latter is frequently associated with the edges of coronal holes where the magnetic field expands super-radially (*e.g.* Wang and Sheeley, 1991), alternative theories have been proposed, including reconnection between closed and open magnetic-field lines that circulate inside coronal holes (Zhao, Zurbuchen, and Fisk, 2009), and recently a network of narrow open-field corridors that map to a web of separatrices and QSLs in the heliosphere (Antiochos *et al.,* 2011) have all been suggested.

Observations using the ACE and *Ulysses* spacecraft have detected *in-situ* evidence for the presence of AR material on AR-associated open field lines (Liewer, Neugebauer, and Zurbuchen, 2004; Ko *et al*., 2006), which in fact can form part of Antiochos and co-workers' QSL-web. This latter point is reinforced by the composition of the slow wind plasma, which is characteristic of the closed field within ARs (Geiss, Gloeckler, and von Steiger, 1995, von Steiger *et al*., 1995). Composition features include the enhanced presence of elements with low first ionization potential (FIP) whose abundances are ≈ four times those of the photosphere (Von Steiger *et al.*, 2000, Feldman and Widing, 2003). By contrast, the fast-wind plasma shows no such enhancement, whereas plasma originating on open field regions rooted on the boundary of coronal holes have a FIP bias that ranges between the FIP bias of the slow and fast solar wind. We note that there is yet no broadly agreed theory of the origin of the FIP effect with many proposed theories that differ largely on the invoked physical mechanism. In addition the rapid fall-off in plasma density with height ensures that the ionization equilibrium established in the lower corona and characterized by a temperature, T_e, remains "frozen-in" to the plasma for distances beyond 1 – 3 R_{Sun}, depending on the atomic element. The ion state populations

established at these temperatures can be measured *in situ* by instruments on spacecraft in the heliosphere e.g. ACE, *Ulysses*. Temperature estimates based on such measurements show $T_e \geq 1.5$ MK for the slow wind as opposed to $T_e \leq 1.2$ MK for the fast component (von Steiger *et al.,* 2001, Zurbuchen *et al*., 2002). In other words, the fast and slow solar wind originate from cold and hot regions of the base of the corona, respectively.

In this article we examine the AR-associated outflows from an AR–CH complex that crossed the solar disc in the period 3 – 18 January 2008 and ask the questions i) what drives them and ii) whether or not these plasma flows contribute to the solar wind. In Section 2 we present a wide range of observations of the AR–CH complex and employ linear force-free modeling to relate the AR upflows to the presence of QSLs. Employing local as well as full-Sun potential-field models we find a high-latitude null-point above one of the ARs and identify the QSLs which contain a separatrix, enabling some of the AR plasma flows to reach the solar wind. In Section 3 we examine the data from the ACE spacecraft for evidence of AR-related plasma in the near-Earth slow solar wind. Finally, we conclude in Section 4.

2. Observations of CH/AR Interaction

Since the peripheral AR outflows are associated with unipolar magnetic field regions and are often adjacent to CHs (Sakao *et al.*, 2007; Harra *et al.*, 2008; Doschek *et al.,* 2008), we identified at the beginning of January 2008 a solar configuration, established during Carrington Rotation (CR) 2065 that appeared favorable for AR outflow studies.

2.1 Overall Coronal and Magnetic Field Configurations

A *Hinode*/XRT image for 07 January 2008 at 10:12 UT is shown in Figure 1. Here, moving from West to East, we can see a section of the quiet corona close to the west limb, followed by a coronal hole labeled CH1. This feature is followed by an AR (NOAA 10980), labeled AR1. A second AR, which remained spotless during its disc passage and therefore was not given a NOAA number (AR2), is located further to the East. It is a small AR since it had a magnetic flux of approximately 1×10^{21} Mx and it is separated from AR1 by an interval of quiet corona. AR2 is situated at the northwestern boundary of a second coronal hole (CH2). The outflow region that we discuss in detail below is located at this boundary. Thus, for the interval 2 – 18 January (CR 2065), CH1 leads AR1 in rotation while CH2 lags AR2. As a result of this configuration, the fast SW outflow from CH1 can, by overtaking and compressing quiet Sun slow wind, create a stream interaction region (SIR1) in the heliosphere. The converse situation, which occurs behind CH1, leads to the creation of a rarefaction region (RF1). Similar structures are created in relation to AR2 and CH2 and are indicated in Figure 1. Our discussion will focus on the AR2–CH2 boundary, though we also analyze the CH1–AR1 boundary in less detail.

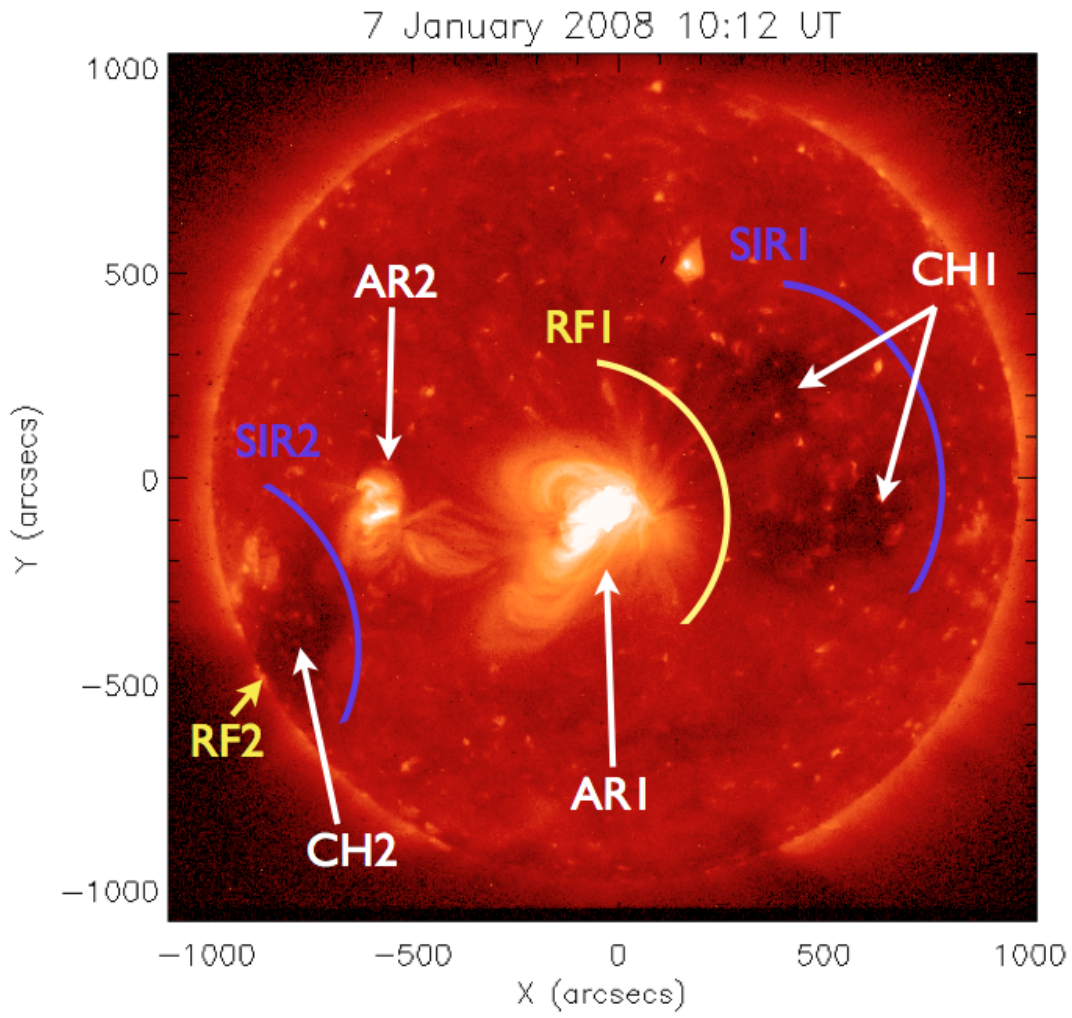

Figure 1. *Hinode*/XRT image for 7 January 2008. **Markings** show a stream interaction region (SIR1), a coronal hole (CH1), a rarefaction region (RF1), and two active regions (AR1 and AR2), followed by a second stream interaction region (SIR2), coronal hole (CH2), and rarefaction region (RF2).

A Carrington map constructed from meridional strips of STEREO/EUVI-B images is displayed in Figure 2a for the complete CR 2065. The yellow arrow indicates the location of the principal outflow site, which is discussed in detail in Section 2.2. The location of the HCS is clearly indicated in the Wilcox Solar Observatory and NSO/Global Oscillation Network Group (GONG) Potential Field Source Surface (PFSS) model shown in Figures 2b and 2c. Comparison of Figures 2a and 2b indicates that during CR 2065, the inward projection of the HCS separates AR1 from AR2. Thus the outflow region of AR2 (yellow arrow), which we discuss in Section 2.2, will arrive at L1 on the Sun–Earth line of sight behind, *i.e.* later than, the HCS crossing. Regions of positive (green) and negative (red) open magnetic field are associated with the coronal holes CH2 and CH1, respectively (compare Figures 2a and 2c). The outflow site observed with EIS is again indicated in Figure 2d where the large area of closed field, shown in blue, is associated with the closed magnetic structures in the streamer belt.

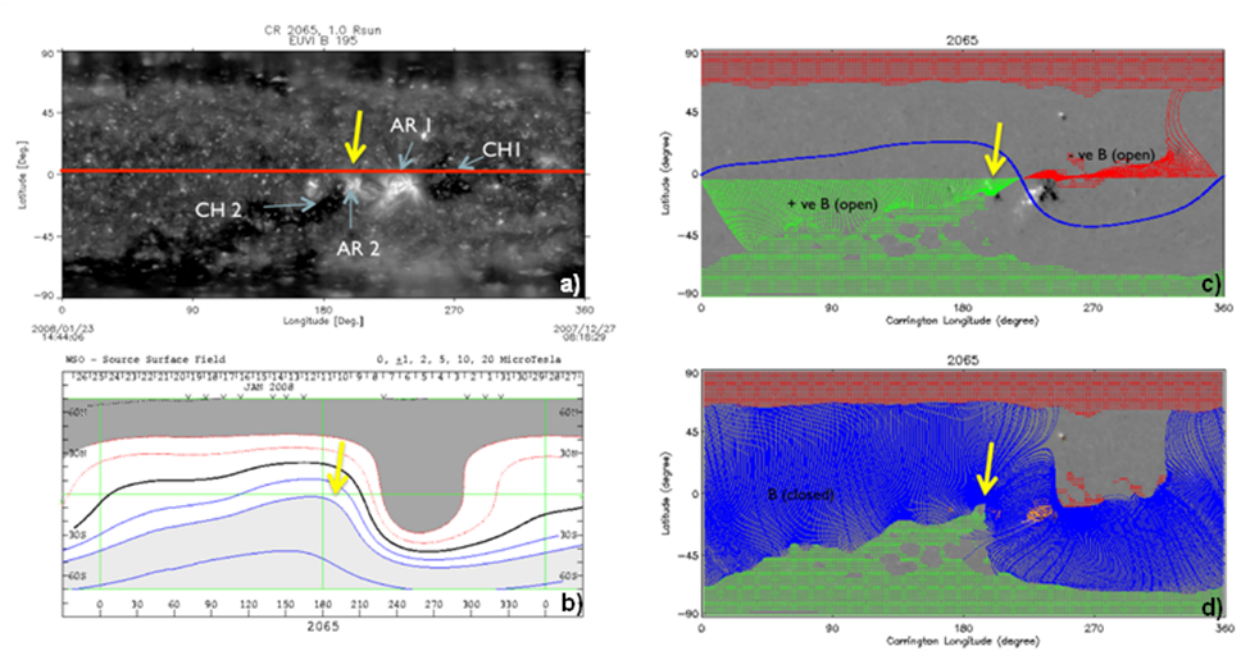

Figure 2. a) Carrington Rotation 2065 displayed with STEREO-B/EUVI images. b) Wilcox Solar Observatory PFSS model for CR 2065 with isocontours of the large-scale radial field component. Grey areas show the open field regions. c) NSO/GONG PFSS model with open field reaching the ecliptic plane (shown up to the source surface at 2.5 R_{Sun}). The AR and CH features shown in Figure 1 are indicated, while the solar Equator is drawn in red. The red/green areas show the negative/positive polarity of the open field regions and the blue line is the inversion line at 2.5 R_{Sun}). d) As for c) but showing the largest closed field lines (reaching 2.5 R_{Sun}). The yellow arrow indicates the studied site of the EIS outflow from AR2.

2.2 Active Region Outflows

A selection of three AR outflow and intensity maps for Fe XII 195 Å emission made for AR2 in the interval 10 – 11 January 2008 is shown in Figure 3. A more complete

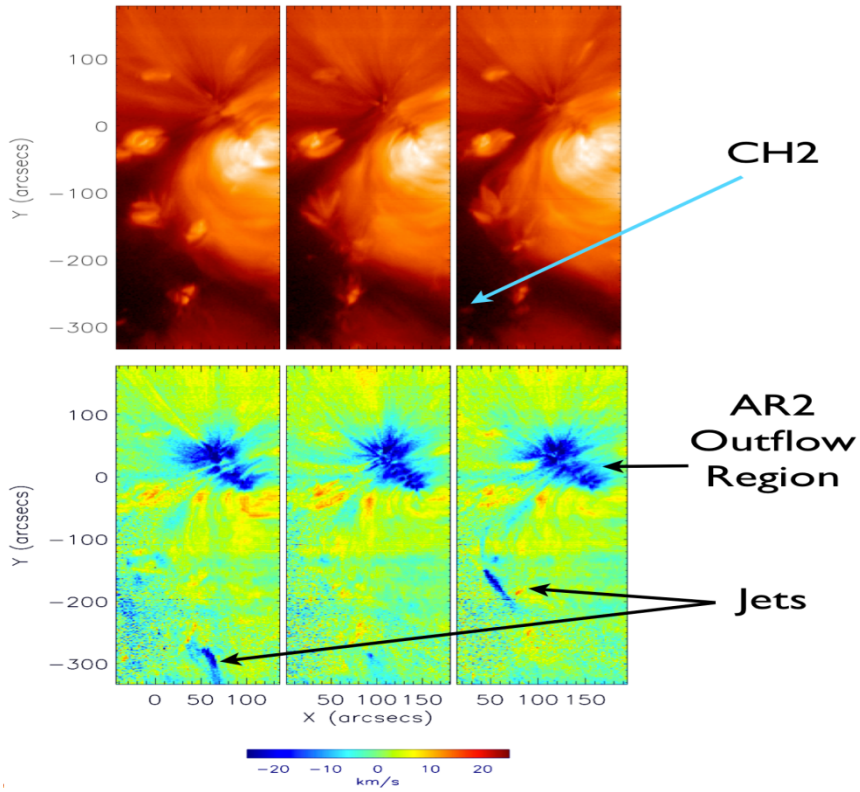

Figure 3. Set of three EIS Fe XII ($T_e \approx 10^{6.1}$ K) intensity maps (top row) and the corresponding velocity maps (bottom row). Reading left to right, maps were obtained on 10 January 2008 at 18:08 UT and at 22:51 UT, and on 11 January 2008 at 00:17 UT. CH2 is indicated in the upper panel while the strong and variable outflow region at the NE edge of AR2 is shown in the velocity maps, as are two coronal jets.

set of maps is available in the on-line material. The EIS instrument observed the mature, dispersed AR2 at 18:07 UT on 10 January 2008 when it was at disc center. Observations continued for approximately three days until 22:08 UT on 13 January 2008. A raster scan using the 2" slit and consisting of 90 pointing positions with exposure time of 25 seconds per position for a total raster time of 37.5 minutes was performed with EIS. The intensity and velocity maps shown in Figure 3 were made from the slit raster observations. The field of view (FoV) is 180" × 512" and covers all of the positive polarity and part of the nearby equatorial CH but does not extend to the leading negative polarity on the western side of the AR. The EIS study included 24 wavelength windows containing more than 50 emission lines, however, the signal-to-noise (S/N) ratio was insufficient in a large number of weaker lines as the study was designed for rapid cadence observations of AR footpoints.

EIS data reduction was carried out using standard SolarSoft EIS procedures. Raw data were corrected for dark current, hot, warm and dusty pixels, and cosmic rays. Relative Doppler velocities were determined by fitting a single-Gaussian function to the calibrated spectra in order to obtain the line centre for each spectral profile. A fitted line centre was further corrected by removing instrumental effects including slit tilt and orbital variation. Blueshifts (redshifts) seen in the final velocity maps correspond to negative (positive) Doppler velocity shifts along the line-of-sight. As indicated in Figure 3, it is clear that the EIS observations show hot-plasma outflows. These are mainly located at a single site on the AR2–CH2 boundary (see Figure 2). The

outflows are variable with line-of-sight velocities in the range 20 – 40 km s^{-1}. There are also significant spatial changes in the extent of the outflow site.

Coronal jet-related outflows are also seen and two examples are indicated in Figure 3. These may be due to small-scale flux emergence with subsequent interchange reconnection within CH2, or at the AR2–CH2 boundary. The coronal-hole boundaries also show significant time evolution. A set of three images for the interval 9 – 13 January is presented in Figure 4 and the corresponding boundary evolution movies are given in the on-line material. CH boundary evolution can contribute to outflows by interaction of open field with closed AR field but, since the eastern boundary of AR2 and CH2 have the same magnetic polarity, classical antiparallel interchange reconnection is less likely to occur for the present configuration and it is restricted to the locations of small-scale flux emergence. Magnetic reconnection between open and closed field lines, even when their photospheric footpoints are of the same magnetic polarity, can still occur when there is a coronal null-point present, *e.g.* in a pseudo-streamer configuration (Del Zanna *et al.,* 2011, Masson *et al,* 2012), or high in the corona at the streamer tip (Wang, Sheeley, and Rich, 2007; Kahler, Jibben, and DeLuca, 2010).

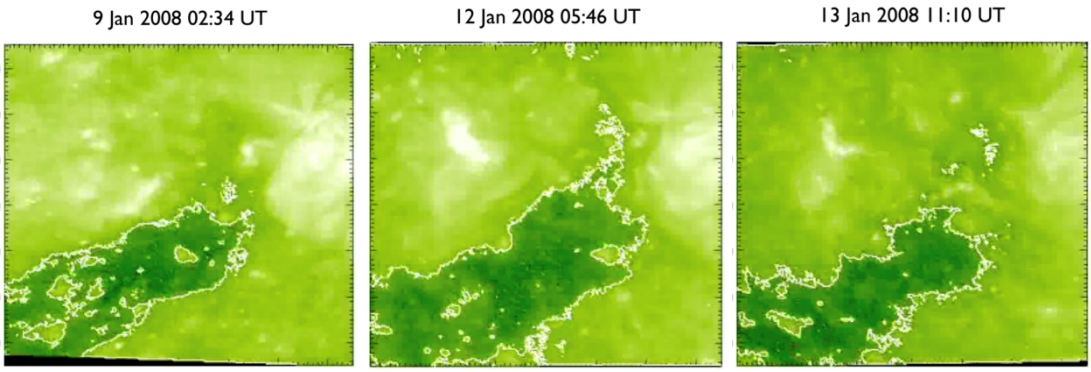

Figure 4.Three individual SOHO/*EUV Imaging Telescope* (EIT) 195Å image frames from a movie covering the interval 9 to 13 January which illustrates the boundary evolution of CH2. Though viewing angles do influence the CH boundaries, the dynamic nature of the CH boundary is evident. The images represent a 700" × 700" area. See the corresponding movies in the electronic supplement to this article in the electronic version both with and without the contours indicating the boundary of the CH.

2.3 Reconnection at Quasi Separatrix Layers - a Likely Outflow Driving Mechanism

Magnetic reconnection is also possible along QSLs. It occurs between same-polarity magnetic field lines (loops) if there is a significant angle between them; such magnetic component reconnection results in footpoint exchange of the two loops. The operation of component reconnection is outlined in Figure 5. Two sample field lines from large low-density and small high-density loops are shown in Figure 5a. Because of the angle between them, the *x*-components are oppositely directed although the *y*-components remain parallel. The oppositely oriented B_x components reconnect resulting in a footpoint exchange between the low-density and high-density field lines. This creates a density gradient in the long loops that leads to an upflow (Baker *et al*., 2009; Bradshaw *et al*., 2011). An opposite gradient in the closed field lines results in a downflow.

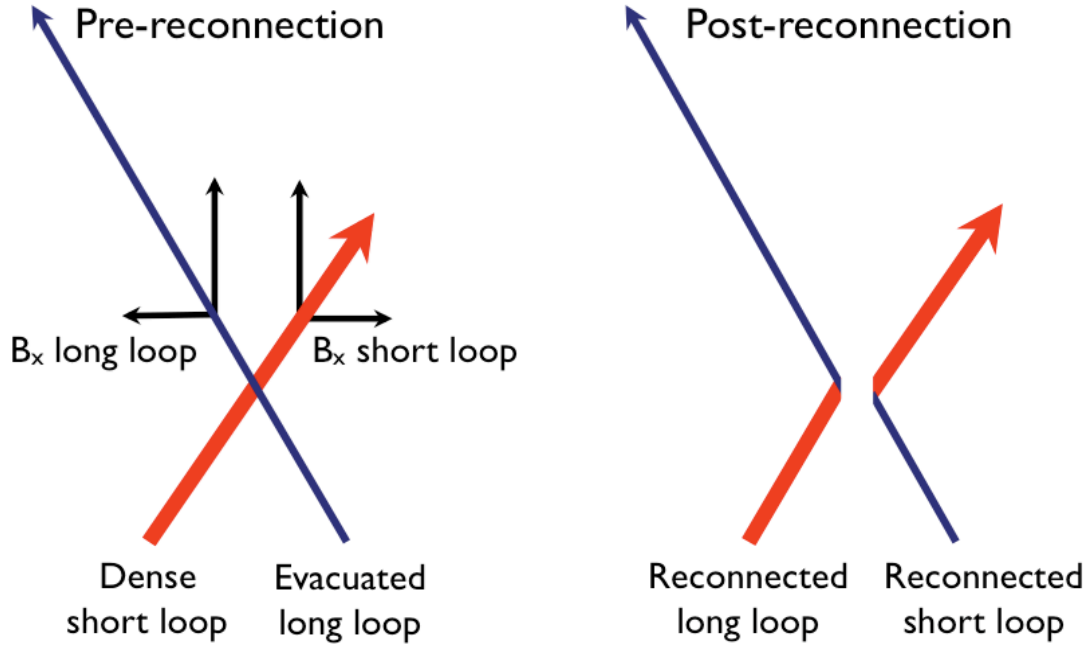

Figure 5. Simplified 2D cartoon explanation of magnetic reconnection between two positive-polarity magnetic loops (field lines) having a non-zero angle between them. This type of magnetic component-reconnection can take place along QSLs at the periphery of an AR, *e.g.* between dense loops of the AR and more evacuated loops connecting elsewhere outside or inside the AR. (Left) Pre-reconnection configuration: the dense closed AR-loop (thick red line) and the evacuated far-closing field line (thin blue line) have an anti-parallel B_x component. Along the QSL between these field lines of drastically different connectivities, a current sheet forms enabling reconnection. (Right) These field lines "break" and reconnect. Far-connecting post-reconnection field line shown on the left will have a dense lower and an evacuated upper part, while the reconnected short field line has densities the other way around. The resulting density gradients drive plasma flows upward on the long field line, leading to blue-shifted plasma flows and downward along the closed loops, leading to red-shifted flows.

2.3.1 *Flows and QSLs*

When viewing examples of peripheral AR outflows observed by EIS, it is clear that in a substantial majority of cases, these flows are found at locations where magnetic field lines with drastically different connectivities meet or are rooted. These locations are called QSLs (Démoulin *et al*., 1996). The role of these sites as drivers of outflows was proposed by Baker *et al*. (2009) based on extensive observations and magnetic modeling of AR 10942, which was visible on the disc from 16 – 28 February 2007. In discussing the outflows from AR2 in the present article, we adopt the approach described by these authors.

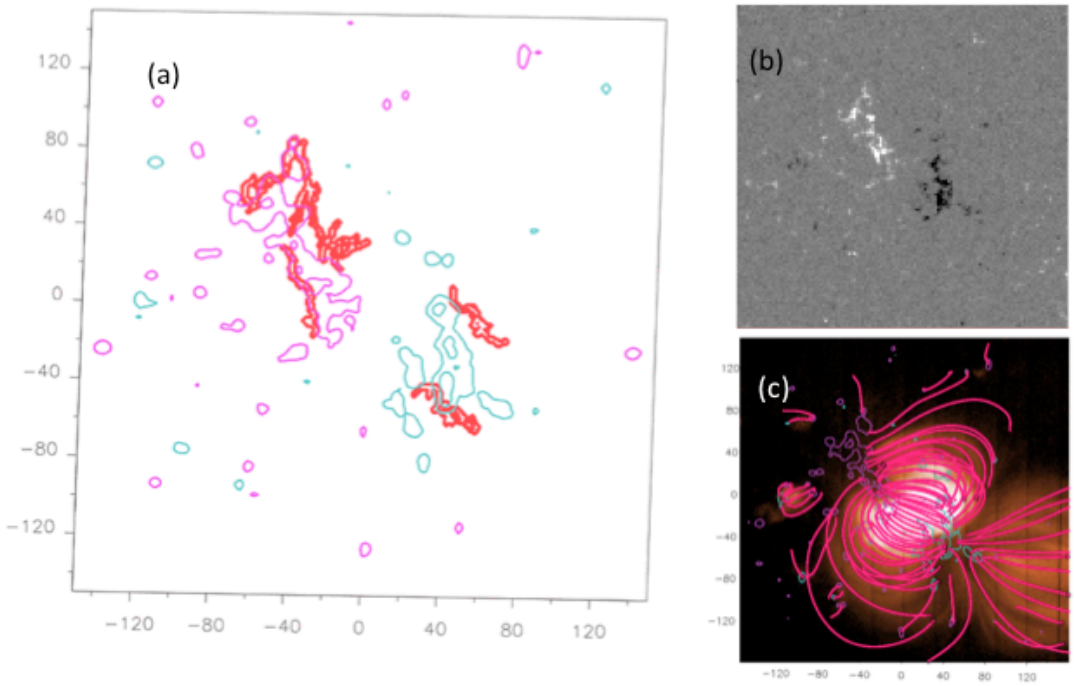

Figure 6. (a) Photospheric trace of dominant QSLs indicated by the thick red lines overlaid on an MDI magnetogram (turquoise /magenta is negative/positive, -50/50 G and -300/300 G contours). The most extended QSL trace is located over the positive polarity of the AR within the EIS FoV. For context, (b) an MDI magnetogram, and (c) an Fe XV image overlaid with field lines from the same LFFF model used for computing the QSLs in panel (a) for AR2 are shown on 10 January 2008.

QSLs are defined by the regions of high values of a function called the squashing degree, or simply Q, which characterizes the locations where the field line mapping to the photosphere shows drastic changes (Titov, Hornig, and Démoulin, 2002). QSLs are both preferential locations for current sheet development and magnetic reconnection (*e.g.* Aulanier, Pariat, and Démoulin, 2005). At the locations, where Q becomes infinitely large, a QSL is simply a separatrix and the field line mapping is discontinuous (see Démoulin *et al.*, 1996). In this case a magnetic null point is present (or field lines are tangent to the photosphere). It was shown by Masson *et al.* (2009, 2012) that a separatrix is surrounded by a thin volume of finite but high-Q values, so a separatrix is embedded in a QSL. This has implications for 3D reconnection: a field line is not reconnecting only once with another field line (as in 2D) but with a continuous set of field lines within a QSL, irrespective of the presence or absence of a separatrix within the QSL. In summary, thin QSLs (large Q values) generalize the concept of separatrices: they are volumes, where reconnection is expected to occur.

2.3.2 *Linear Force Free Model of AR2*

The results of a linear force-free field (LFFF) magnetic extrapolation were used to establish the locations of the QSL traces shown in Figure 6. Although the EIS FoV does not include both polarities of the AR, this is not crucial for an analysis of the AR2 outflows, since the coronal extrapolation is calculated using the full-disc MDI magnetogram closest in time to the relevant EIS observation, and QSLs are defined by the global properties of the magnetic field. The LFFF extrapolation of the coronal field was compared with an EIS Fe XII slot raster image taken at 16:02 UT on 10

January 2008. Good agreement between the modeled loops and the real coronal structures of the AR is achieved with $\alpha = 3.1\times10^{-3}$ Mm^{-1} (*cf.* the extrapolations overlaid on a Fe XV image in Figure 6c). The low α value implies that the AR is weakly sheared. This is confirmed by inspection of larger images containing both polarities.

Figure 6 shows the photospheric trace of the dominant QSLs with SOHO/*Michelson Doppler Imager* (MDI) magnetic-field isocontours of 50 G and 300 G. The most extended QSL trace is located over the positive polarity of the AR within the EIS FoV. Two other QSL traces are found over the AR's negative polarity, just outside of the EIS FoV. It should be noted that the identification of dominant QSLs is difficult in this case because AR2 is fragmented and dispersed, therefore, creating numerous small QSLs. Only QSLs with Q exceeding a minimum threshold of 10^7 are designated here as dominant. It is noteworthy that the highest value of Q found in our computation is $Q \approx 10^{36}$. This upper limit is set by the numerical limitations obtained in computations with double precision of the field lines. Such QSLs are so thin that they are expected to behave physically as separatrices.

The Fe XII intensity and velocity maps for the following positive polarity section of AR2 are displayed in Figures 7a and 7b. They were made at 18:07 UT on 10 January 2008. The overlay image (Figure 7c) shows that the strong AR outflows seen in the EIS velocity map are spatially coincident with field lines having footpoints in the neighborhood of the QSL located over the positive polarity

In our LFFF model, there are a number of field lines, that leave the 3D box shown in Figure 7c (a portion of the computational box): these end with a circle and are drawn in orange. The LFFF hypothesis is not well suited for modeling "open" (or very extended) field lines because the large-scale magnetic field lines are unrealistically distorted. Moreover, the photospheric field is forced to be balanced within the computational box that, in this case, is taken as large as 600 Mm in all three spatial directions, so including both AR2 and AR1. The original imbalance in our magnetic-field data was approximately 1 G, when uniformly distributed in the above computational box. This implies that the magnetic field computed in weaker field regions, away from the AR, is questionable.

Even with the constraints mentioned above, we find a magnetic null point between AR2 and AR1 at a height of about 120 Mm. It is nearly a 2D null, *i.e.* the field lines in the vicinity of the null point are nearly planar, with a ratio of the smallest to the largest eigenvalue of the field-gradient matrix in the fan is ~ 0.05, meaning that one component of the field is only about 5% of the other one in the fan plane (*e.g.,* Lau, 1993, for a study of null points and the definition of the eigen vectors and eigen values). Such types of null have been found previously in several solar configurations (*e.g.* Mandrini *et al.*, 2006; Luoni *et al.,* 2007). This implies that the magnetic field remains very weak when going away from the null along one specific direction (defined by the eigenvector of the lowest eigenvalue). This configuration is due to the two nearly parallel magnetic bipoles of AR2 and AR1. A fan separatrix is associated with the null point. The set of orange field lines present in the upper part of Figure 7c is indeed drawn in the immediate vicinity of this separatrix. We also verify that Q reaches in this region the highest possible values according to our integration

precision. Then, we propose that the blue flows observed in this specific region are related to continuous magnetic reconnection at the null point as proposed by Del Zanna *et al.* (2011), but so far without knowing whether or not it involves open field lines.

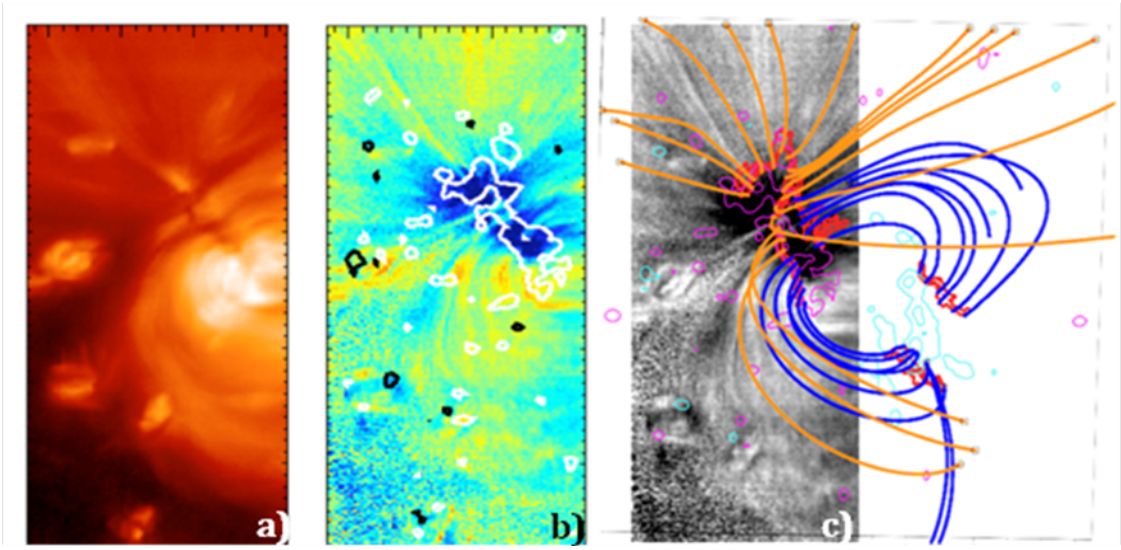

Figure 7. a) EIS Fe XII intensity map of AR2. b) Fe XII velocity map overlaid with ± 50 G MDI magnetic contours. White/black is positive/negative polarity. c) Photospheric trace of QSLs (thick red lines) and field lines originating in the QSLs computed from a LFFF extrapolation. They are overlaid on a grayscale EIS Fe XII emission line velocity map. Orange/blue field lines are drawn from the QSL over the positive polarity. Lines with circles leave the viewing 3D box and are considered to be open or large extended loops. Magnetic field isocontours are shown in continuous magenta/turquoise lines for positive/negative values of the field (± 50 G and ± 300 G).

2.3.3 *Local and Full-Sun Potential Field Models*

The LFFF model in the previous sub-section was constructed to take account of the weak magnetic shear present in AR2. However, on larger scales the magnetic field is typically closer to a potential field. To establish whether or not the previous high-altitude null point is a bias of our LFFF modeling, we compute the nulls in the AR1–AR2 complex in the potential approximation. For this modeling, we enlarged our computational box to 1600 Mm in both east – west and north – south directions both to decrease the influence of the lateral boundaries and to remove the flux unbalance (which corresponds to 0.03 G per pixel).

With this potential field, the null point shifted upwards and West by about 10 Mm, and South by about 56 Mm. This shift is mostly in the direction of the eigenvector with the lowest eigenvalue, as expected (Démoulin, Hénoux, and Mandrini, 1994). However, the separatrices have a much smaller shift of position (the null is mostly moving along the so-called separator, the intersection of separatrices). The spine and field lines passing in the vicinity of the null point are shown in Figure 8. A comparable figure is found with the LFFF extrapolation. The photospheric trace of the separatrix is slightly shifted (and rotated) in the following polarity of AR2 (compare Figure 7c to 8b). The same is true with the QSLs; this is an expected result since all our previous studies (*e.g.* Mandrini *et al*., 1996; Démoulin *et al*., 1997) have shown the structural stability of QSLs when the magnetic field is not drastically

modified (as in this case, given the low value of α).

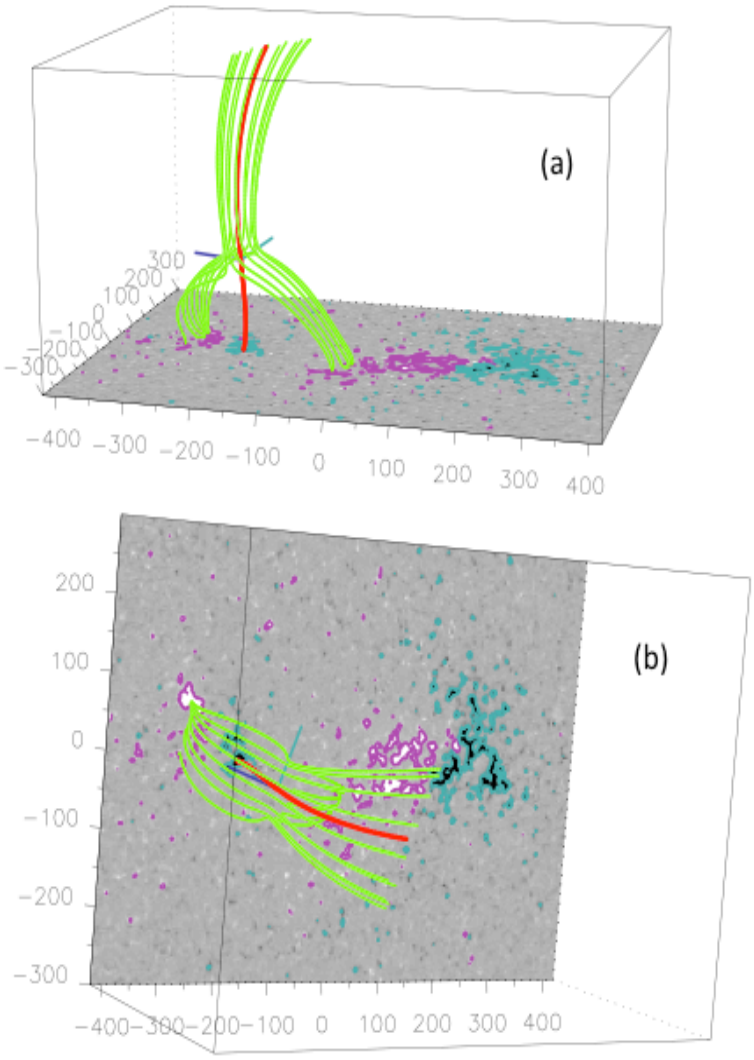

Figure 8 Location of a high-altitude (about 130 Mm) null point above AR2 in the AR1-AR2 complex in a Cartesian potential field extrapolation. The spine field line (red) and fan field lines (green lines) are shown from two perspectives (a) from the South and (b) as seen from Earth. The bottom boundary is an MDI magnetogram taken on 9 January 2008, when the AR1–AR2 complex was closest to the central meridian. Negative polarity is contoured with turquoise, positive with magenta.

To check if the spine field line originating from the null shown in Figure 8 extends up to the source surface, we carry out Potential Field Source Surface (PFSS) modeling of the whole Sun. This global modeling is complementary to our previous more local models since it takes into account the larger scales. The surface-field maps that are used in calculating the PFSS model are sampled from an evolving-flux model, and not from the usual synoptic map. The main difference is that the surface-field is not static when it is not visible form Earth; instead the field is sheared due to the differential rotation, advected poleward due to meridional flows, and undergoes dispersal due to the convective–supergranular motions. The evolving scheme is presented by Schrijver and Title (2001) and the method by which data are inserted into the model is discussed by Schrijver and DeRosa (2003). As we are mostly interested in the AR2–CH2 interface, the model is optimized for its central meridian location (11 January

2008, 00:00 UT) by building a synoptic map centered on this time. The model is shown in Figures 9 and 10 as viewed from the Earth on the 11th (AR2 is at central meridian) and 6th January, respectively.

Figure 9c shows large-scale topological features, *i.e.* separatrix surfaces, null points above 1.02 R_{Sun} (14 Mm) and their spine field lines in the solar corona (cyan lines) up to the source surface or closing elsewhere on the Sun at a distance. Each of these null points has a separatrix surface associated with it. The intersections of these separatrix surfaces with either the upper (if it reaches the source surface) or lower boundary of the domain are indicated with red lines. AR1 and the eastern-most part of AR2 are under the yellow-colored semi-transparent streamer separatrix surface flanked by the two CHs (Figure 9d). This separatrix is between open and closed field and is defined from the inversion line present on the source surface at 2.5 R_{Sun} (thick blue line in Figure 10b). This is identified with the base of the HCS, which is located typically within the Heliospheric Plasma Sheet (HPS). Finally, the grey areas at the photospheric level are the footprints of open flux as determined by the PFSS model.

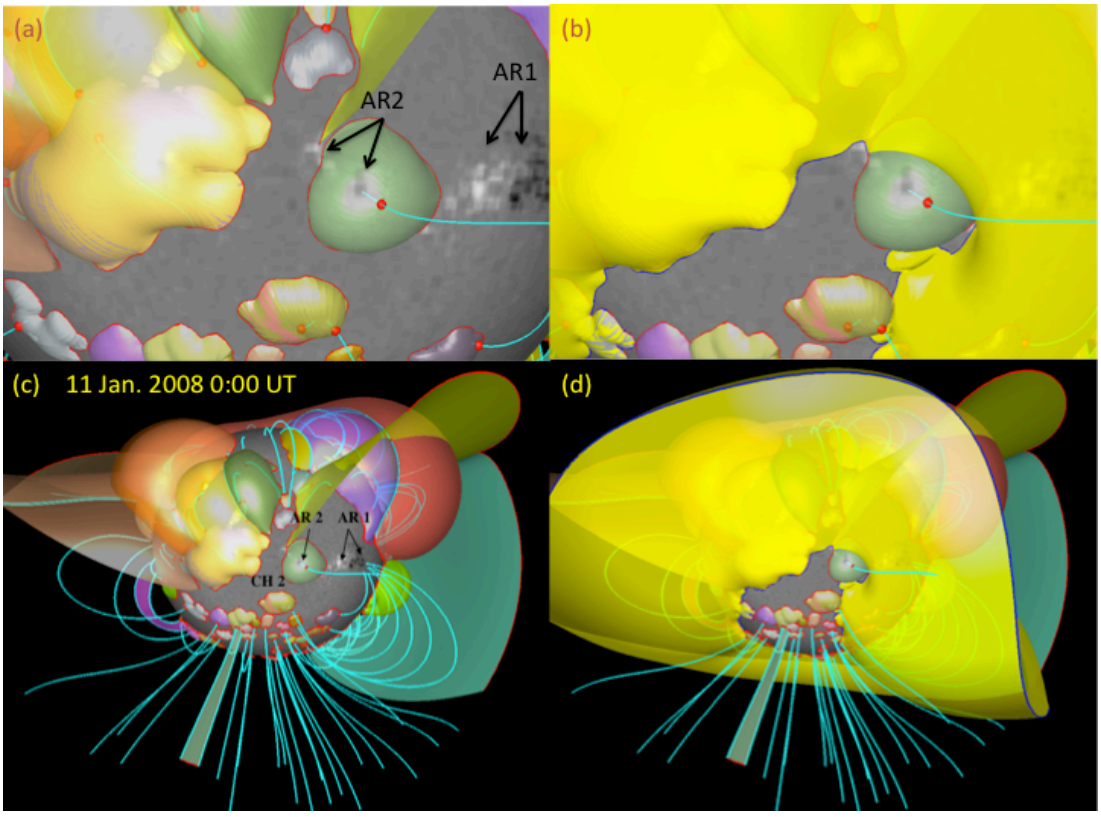

Figure 9 PFSS extrapolation and topological structures of the solar corona for 11 January 2008 with the locations of AR1, AR2, and CH2. The main topological features are streamers, pseudo-streamers, null-points, and their associated fan surfaces and spine field lines. The various semi-transparent colored surfaces are separatrices. The null points are indicated with red dots and the spine lines are the cyan lines associated with these nulls. Thick red and blue lines, indicating pseudo-streamers and streamers, respectively, delineate the intersections of the separatrix surfaces with the photosphere and with the source surface. Panels (a) and (c) are without, while (b) and (d) are shown with the (yellow semi-transparent) streamer separatrix surface. The panels (a) and (b) are zoomed-in details of (c) and (d), respectively. AR2 is partially under a fan surface associated with the null point (red dot), also shown in Figure 8. This fan surface is only partially enveloped by the (yellow) streamer surface. Part of the positive (trailing) polarity of AR2 is in the open-field region of CH2.

Figure 9a shows that AR2, in accordance with the modeling illustrated in Figure 8, has indeed an associated null point and the separatrix dome (fan surface, colored in green) covers nearly the entire AR2, but for the easternmost part of its following (positive) polarity. This separatrix dome is not entirely under the streamer (Figure 9a, b) and the null point and its spine field line, which extends up to the source surface (see Figure 10a), are in the "open-field" domain east of the streamer. On the other hand, AR1 seems to be almost fully under the streamer and has no associated null point, but several spine field lines closing on its southwest leading (negative) polarity (Figure 10a).

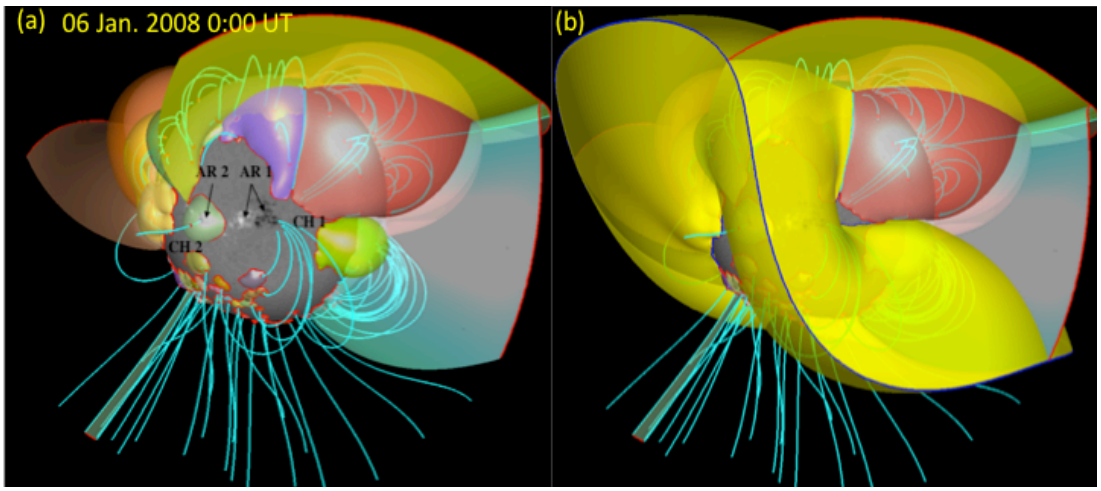

Figure 10 PFSS extrapolation and topological structures of the corona as viewed from the Earth on 6 January 2008 with the location of CHs and ARs indicated. The main topological features are streamers, pseudo-streamers, null points and their associated fan surfaces and spine field lines. They are represented with the same drawing convention as in Figure 9. Panel (a) shows the model without and (b) shows it with the yellow semi-transparent closed-loop streamer region associated with the source-surface inversion line (thick blue line at a radius of 2.5 R_{Sun}). AR1 is nearly fully enclosed by the main streamer, while AR2 has a pseudo-streamer associated to the null point.

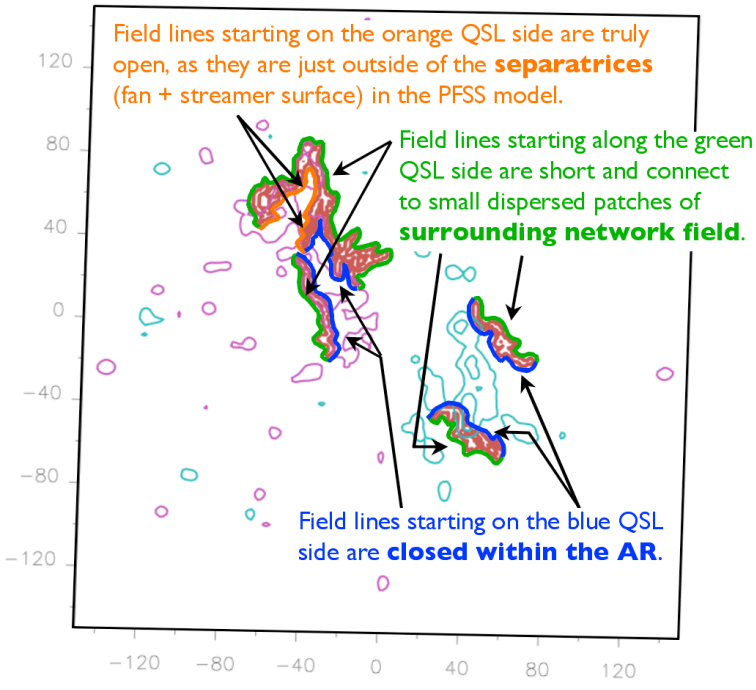

Figure 11. QSL locations in AR2 (*cf.* Figure 6 where QSLs are shown in dark red/brown) with the types of connectivity on both sides color-coded and the characteristic connectivities described using the insight gained from PFSS modeling. The QSLs are overlaid on an MDI magnetogram where isocontours of the polarities are represented with different colors (turquoise is negative, magenta is positive polarity). Different sides of each QSL are coloured according to the field line connectivity found.

2.3.4 *Detailed Analysis of QSLs within AR2*

The connectivities of the dominant QSLs in AR2 are displayed with detailed explanations in Figure 11. Sites where field lines originating at the QSLs connect within/outside of the AR are indicated by the blue/green and orange color scheme around the dark red (or brown) QSL traces, as follows. Field lines starting along the "outside" of the QSLs, marked by thick green lines, are short loops that connect to the small dispersed magnetic fragments of the surrounding network field. These field lines are not displayed in Figure 7c (since they are not linked to the blue-shifted upflows). Thick orange lines over the positive polarity show where the open field lines drawn in Figure 7c are rooted on the "inside" of the main QSL. Such field lines are going to large heights in the Cartesian LFFF and potential-field extrapolation, passing in the vicinity of the null point (Figures 7c and 8). The full-Sun extrapolation shows that they are open (Figures 9 and 10). Finally, field lines starting on the "blue" side of the QSLs are closed within the AR and connect the AR's opposite polarities (see blue field lines in Figure 7c). A combination of information on the footpoints of field lines enveloping the fan surface and the intersection of the separatrix enveloping the streamer with the photosphere shown in Figures 8, 9, and 10 enables us to confirm that the field lines seen in Figure 7c leaving the 3D box are indeed open and their associated QSLs are, in fact, separatrices.

The QSL locations and field-line connectivities are important for understanding the outflows that originate in the vicinity of the QSLs and extend into the corona. As shown in Figure 7c, the outflows occur both along "open" (drawn in orange) and closed field lines (drawn in blue) that are rooted at the dominant QSLs. The magnitude of the flows is comparable in both cases. This both supports reconnection within QSLs, as proposed by Baker *et al.* (2009) and reconnection associated with a magnetic null point, as proposed by Del Zanna *et al*. (2011). In both cases the flows are expected to be driven by the over pressure present in the shorter of the pre-reconnection loops, driving an upward flow in the longer of the two reconnected loops, as modeled by Bradshaw *et al.* (2011). In the case of an open field reconnecting with a closed field, this strong asymmetry in plasma pressure is always expected, while in the case of closed-closed reconnection, it is present only when the loops have a marked geometrical and heat-content difference. Provided the asymmetry in plasma pressure is large enough, one expects that the driven flows can be of similar magnitude as in the open field. Such a conjecture remains to be quantified by numerical simulations.

For the reconnection aspect, 3D reconnection with a null point is indeed similar to that without a null point (but with thin enough QSLs), as the fan and the spine of a null point are surrounded by a QSL with finite Q values. This is the case both with closed fields (with Q defined by the field line mapping to the photosphere, Masson *et*

al., 2009) and with closed-open fields (with the mapping to both the photosphere and the source surface, Masson *et al.,* 2012). Indeed for the local reconnection physics, the case with open-field lines is comparable to the closed case with very long field lines. Moreover, 3D magnetic reconnection does not only occur at the null point, like in 2D reconnection, but it involves the slippage of the field lines within the QSL both before and after field lines cross the separatrix. Without a separatrix, 3D reconnection simply occurs only in the slipping mode.

Finally, the PFSS modeling enables us to see which upflows are generated along field lines, which reach the source surface and, thus, are able to channel plasma flows into the solar wind. As a next step, we analyze the SW parameters related to the AR–CH complex.

3. Interplanetary measurements

3.1 Possible Contribution of AR Outflow to the Slow Solar Wind

The solar features (ARs, CHs, flows) that we are discussing are indicated on a *Hinode*/XRT image for 10 January (Figure 12) at a time when AR2 and its associated outflow site are at central meridian. The location of the HCS projected radially on the Sun is also shown based on NSO/GONG PFSS computations. In temporal order, AR1 crosses central meridian on 7th January (see Figure 1), followed by the HCS embedded in the HPS, AR2 with its associated outflow region to the East and finally CH2. About three-four days later than the central meridian passage of AR1, ACE *in-situ* sensors should begin to register plasma of slow SW composition with contributions from the quiet Sun and any outflows associated with AR1. The HPS passage should lead to the detection of material associated with the streamer belt. Foullon *et al.* (2011), in an extensive study of the HPS during this period, have found evidence for plasmoid ejection possibly related to an ICME and a long-decay flare in addition to the presence of streamer material. Analysing another series of events, Rouillard *et al*. (2010a,b; 2011) tracked the outflow of small-scale transients in the heliospheric imagers from the Sun to 1AU and identified the presence of small-scale mangetic-flux ropes embedded in the HCS and near the heliospheric plasma sheet. Then, the HPS should be followed by a plasma of mixed slow wind composition involving streamer belt-related material with a possible contribution from the AR2 outflow. Finally the ACE instruments should register fast SW plasma from CH2.

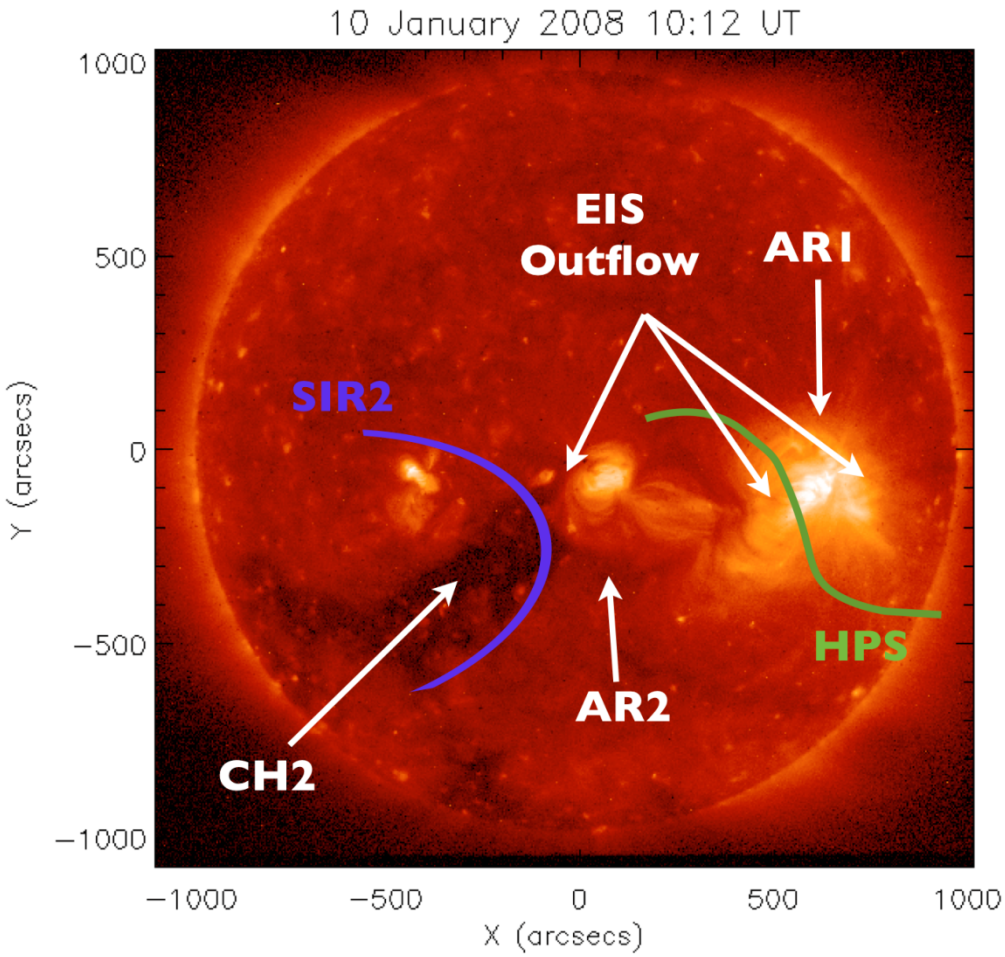

Figure 12. *Hinode*/XRT image for 10 January 2008. Both active regions (AR1, AR2), the second coronal hole (CH2), and stream interaction region (SIR2) are indicated. Also shown are the positions of the active-region outflow sites observed with *Hinode*/EIS and the Heliospheric Plasma Sheet (HPS) location projected radially on the Sun.

In situ observations obtained by ACE for the plasma flow encountering the spacecraft include the ratios Fe/O, O^{7+}/O^{6+}, C^{6+}/C^{5+}, and He^{2+}/H^{+} (*Solar Wind Ion Composition Spectrometer* (SWICS): Gloeckler *et al.,* 1998) along with proton density, temperature, and velocity (*Solar Wind Electron Proton Alpha Monitor* (SWEPAM): McComas *et al.,* 1998). These quantities are plotted against time for the interval 9 to 15 January 2008 in Figure 13. In order to facilitate the comparison with the solar structures the time is running from right to left. The interval for the HPS crossing has been established mainly from the enhanced proton density (see Foullon *et al.,* 2011, for more details). Within the HPS, the HCS location is established from the magnetometer data (*Magnetic Field Experiment* (MAG): Smith *et al.,* 1998). This provides a useful reference for linking ACE to the solar surface.

We start our description of the data on 9 January with a fast wind associated with CH1. The speed progressively decreases inside a rarefaction region to typical slow SW speed before the HPS (Figure 13). After the HPS, a broad peak in plasma velocity is present (around 13 January), well before ACE clearly registers plasma with high-speed SW properties coming from CH2. The velocity peak is associated with a similar peak in the proton temperature. Since both parameters have been found to be related in the SW (*e.g.* Elliott *et al.,* 2005, and references therein), we plot in red the

expected temperature, as well as the range of observed values under typical SW conditions (dotted lines), derived froma scatter plot of observed and measured solar wind speed measured between January 2007 and Januar- 2008. In this scatter plot, we have carefully selected intervals when the solar-wind speed did not change over several days, thereby removing the effect of rarefaction and compression regions. This demonstrates that the observed peak in proton temperature is significantly higher than expected from the peak of the observed velocity. We interpret these results as due to the presence of an important outflow, most plausibly coming from AR2 and associated with a significant extra-heating of the plasma.

The *in-situ* O^{7+}/O^{6+} and C^{6+}/C^{5+} ratios provide another diagnostic of the plasma temperature in the corona, since these ratios are supposed to be fixed values within the SW (because of low collisions at larger distances). The frozen-in height of both is about 1.1 – 1.2 R_{Sun} (*e.g.* Owocki, Holzer, and Hundhausen, 1983). Figure 13 shows that both CH1 and CH2 associated regions have low ratios as expected (dotted line). Higher ratios are associated with the AR1 passage and even larger ones with AR2. Indeed, AR1 is located behind a large streamer region (Figure 9); so, at most the largest scales, which are also typically the coolest, can have a contribution to the SW (by interchange reconnection). On the contrary, AR2 is only partly below the streamer and interchange reconnection involves loops closer to the AR core, so hotter ones. We conclude that the O^{7+}/O^{6+} and C^{6+}/C^{5+} ratios are organised with PFSS derived distribution of magnetic-field strengths at the base of the corona (as found by Wang, Ko, and Grappin, 2009). We further note that there is no peak, but rather a decrease, in these ratios associated to the peak present in proton temperature (around 13 January). This implies that the plasma was not significantly heated in the low corona (*e.g.* by reconnection at the null point), but latter on (*e.g.* by dissipation of Alfvén waves or MHD turbulence).

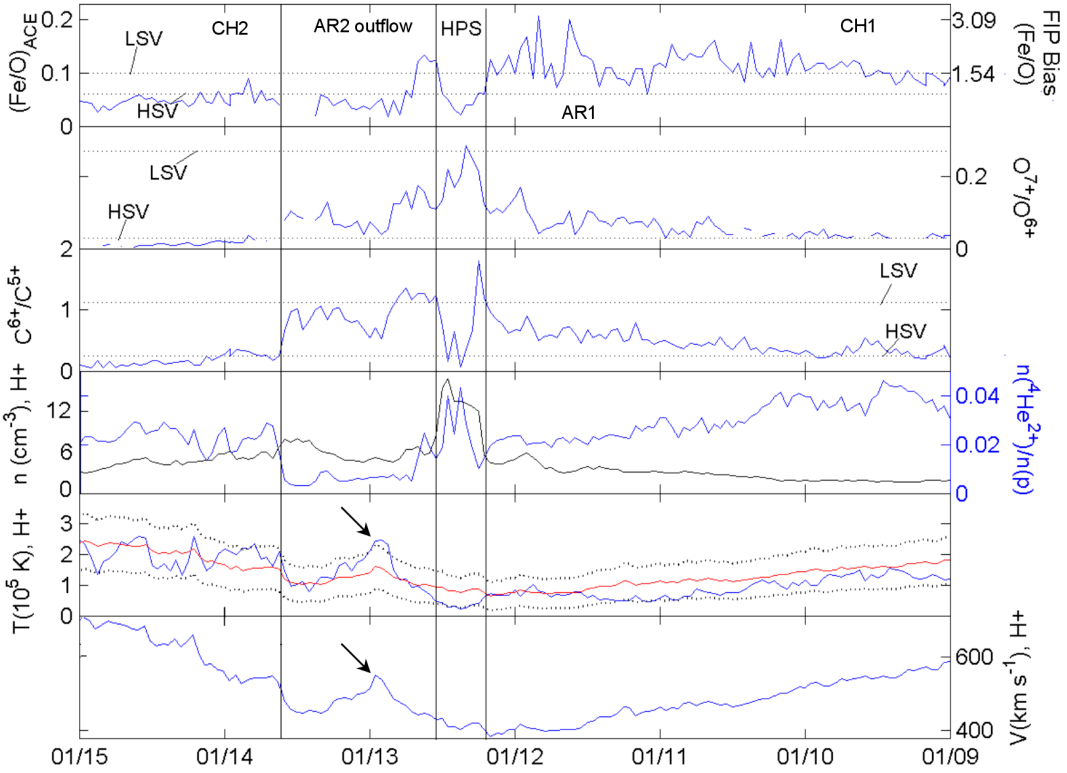

Figure 13. ACE *in situ* observations of SW plasma for the interval 9 – 15 January 2008 (right to left). From the top of the figure, values of the concentration ratios Fe/O, O^{7+}/O^{6+}, C^{6+}/C^{5+}, and He^{2+}/H^{+}, and density, temperature, and proton velocity are plotted against time. The FIP bias, *i.e.* Fe/O normalized to photospheric value, is indicated on the top right. In the three top panels the typical low and high speed values (LSV and HSV) are indicated by the horizontal dotted lines. The expected temperature in a SW with the same velocity is shown in red, while dotted lines show the typical extreme values in the T panel. Passage of the HPS is indicated as are those of CH2, AR2, AR1, and CH1. The black arrows show a proton-velocity and temperature peak, which we link to outflows from AR2.

The Fe/O ratio shown in the top panel of Figure 13 is characteristic of a FIP bias when normalized to the photospheric ratio (shown on the right-hand scale). A FIP bias larger than one should come from the chromosphere where the low-FIP elements are ionized but the high-FIP ones are still neutral (von Steiger *et al.,* 2000; Feldman and Widing, 2003). It has been suggested that by diffusion across the magnetic field, the high-FIP elements can escape from the heated and over-pressurised loops but not the low-FIP elements, implying an enhancement in low-FIP elements of the loops. Because it involves diffusion, such a process requires the storage of the recurrently heated plasma during a period of days to weeks. This is not the case in CHs, and indeed the region associated with CH2 shows such typical value of the fast SW (top panel of Figure 13). The diffusive interpretation faces two surprising observations. The region associated with CH1 has a FIP bias comparable to slow SW conditions, as in the region associated with AR1. The occasional presence of high FIP bias in fast solar wind was noted by Wang *et al.* (2009). This could be related to the presence of faint coronal loops within CH1 as observed with the EUV Imager (EUVI) (see attached movie). Even more surprisingly, the AR2 region has the lowest of the FIP bias values. AR2 is at least one rotation younger than AR1, being first seen on 2 January 2008 (by STEREO-B), while AR1 was observed for the first time on 04 December 2007 on the east limb in the growth stage (also by STEREO-B). Even if

AR2 is younger than AR1 by about one solar rotation, such that diffusion has less time to operate, these low values remain to be explained.

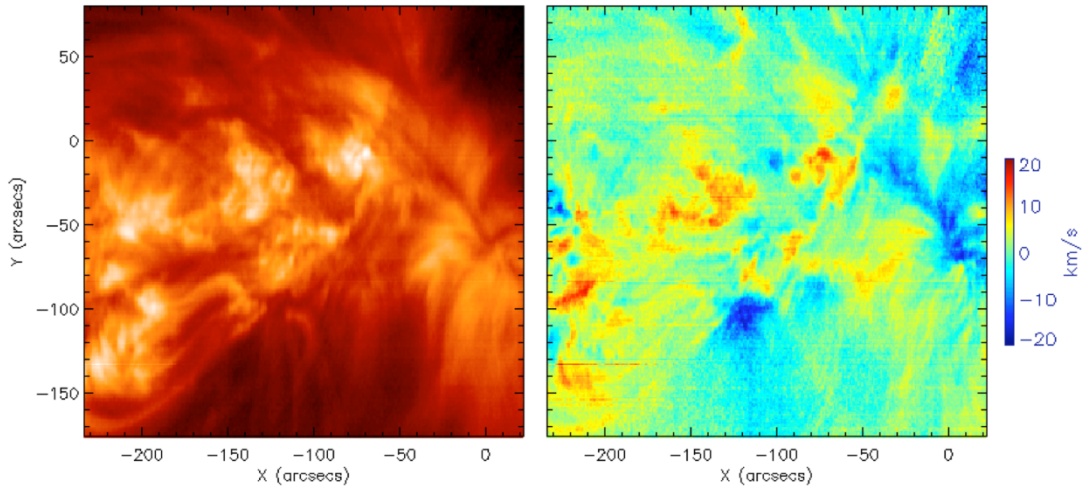

Figure 14. Sample EIS Fe XII intensity (right) and velocity (left) map obtained for AR1 on 6 January 2008 at 23:16 UT. Significant outflows are still visible though with diminished footprint compared to the observations of Brooks and Warren (2011) made for this region on the previous solar rotation.

3.2 Does AR1 Contribute to the Solar Wind?

In contrast to AR2, evidence for contribution by AR1 to the SW is sparse since the peaks in the proton temperature and velocity, observed before the HPS, are much weaker than those associated with AR2 (Figure 13). Moreover the FIP bias is comparable to that in the CH1 region. Still, there is a weak increase of the O^{7+}/O^{6+} and C^{6+}/C^{5+} ratios compared to the nearby plasma originating from CH1. Therefore, below we analyze coronal data to see whether or not there is any evidence that AR1 could be related to plasma outflows.

We have observed AR1 with EIS in a 24 hour interval from 5 to 6 January, 2008. Figure 14 shows Fe XII 195 Å intensity and velocity for one of the 15 observations. Upflows are seen in both the East and the West of the region, although with much diminished footprint area compared to those observed by Brooks and Warren (2011) on the previous rotation. However, as shown in Section 2 for AR2, coronal upflows can be present in closed or open field lines, so that the observation of EIS upflows is not by itself sufficient to make the link with the SW.

The PFSS model of Figures 9 and 10 does show that AR1 is fully inside a large scale streamer. However, this computation assumes a fully relaxed (potential) magnetic field apart from the presence of an imposed source surface, which locally forces the magnetic field to be open. The PFSS model also includes only the large scales without temporal evolution. Using STEREO/EUVI data, we indeed verify that the large-scale observed structures (CH1, CH2, AR1, AR2) are globally reproduced by the PFSS model. However, the EUVI observations also show that both closed and open-like loops are present on the western side of AR1 (Figure 15). The open-like structures are more evident closer to the limb due to a more favourable projection and fewer back/foreground stuctures. Moreover, outflows are present (see attached

movie). We conclude that, while most of AR1 field is closed, there is still a small fraction of open loops present in the leader polarity. This is consistent with the weak signature of AR-related plasma in the SW before the HPS.

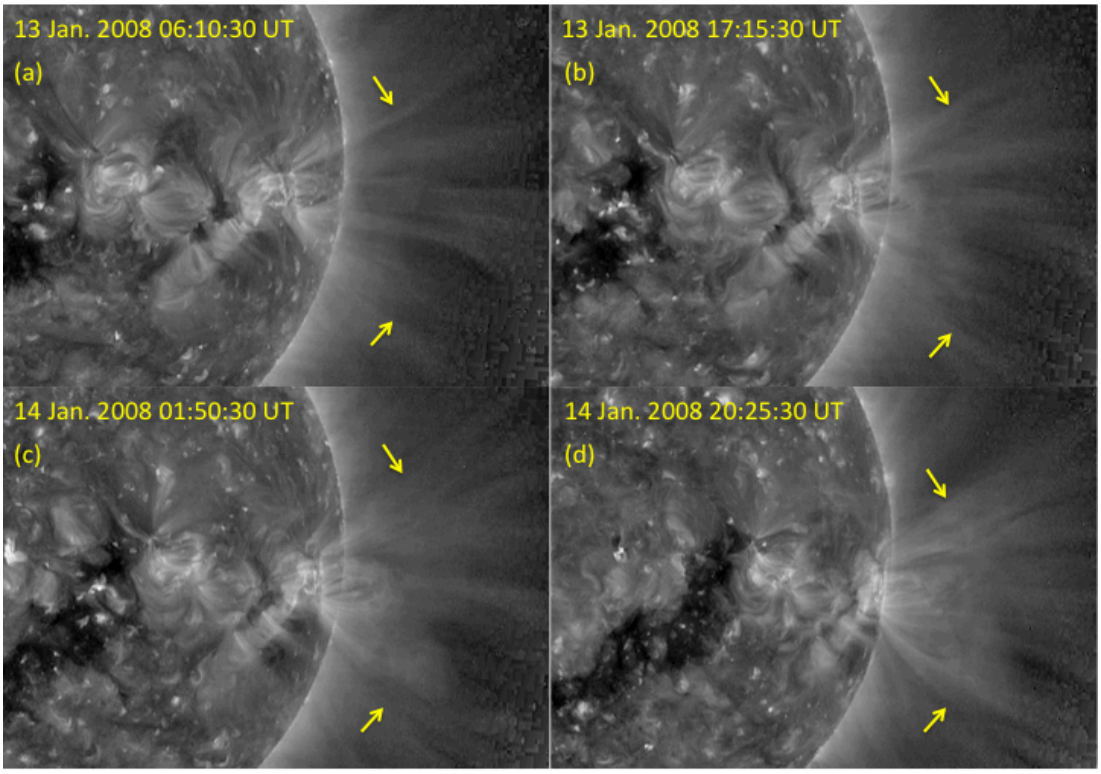

Figure 15 STEREO-A 195 Å EUVI images of the AR–CH complex showing loops fanning out of AR1. These loops become increasingly visible as AR1 approaches the limb. Though PFSS modeling indicates that AR1 is fully enveloped by the streamer above it, the dynamically changing loops fanning out of the AR1–CH1 interface indicate that the boundary is not simple and there is a continuous interchange reconnection process, taking place low in the corona driving brightness changes in the fan. The frames shown here have been wavelet-cleaned and enhanced to extend the visibility of the coronal features as far out as possible above the limb (see Stenborg, Vourlidas, and Howard, 2008, for a description of the method). See the corresponding movie in the electronic supplement to this article in the electronic version.

Finally, we emphasize how the general SW plasma characteristics on both sides of the HPS (CH1–AR1 and AR2–CH2) differ. This illustrates the different kinds of interactions of AR1 and AR2 with open fields. The pre-HPS characteristics appear to be consistent with the outer part of AR1 interacting with the nearby open field. Then, interchange reconnection at large heights is compatible with the relatively low frozen-in temperature observed *in situ*. On the contrary, the post-HPS charateristics are compatible with interchange reconnection at the null and surrounding QSLs at lower heights above AR2, resulting in higher frozen-in temperatures. A more detailed study of the topology of AR1 and the connections between coronal outflows and the solar wind will be carried out in a follow-up article (Mandrini *et al.,* in preparation).

4. Discussion and Conclusions

In this articlewe make an attempt to provide answers to the following questions: what drives plasma upflows observed in ARs with *Hinode*/EIS and whether or not these upflows become outflows forming part of the slow solar wind. We analyse a complex of two ARs (AR1 and AR2) flanked by two CHs (CH1 and CH2) of opposite magnetic polarity (Figures 1, 2) using observations from *Hinode*/EIS and XRT, SOHO/MDI and EIT, as well as STEREO/EUVI.

We employ linear force-free field (LFFF) and potential modeling of the two ARs and confirm previous results by Baker *et al.* (2009) that plasma upflows observed by EIS emanate from the vicinity of narrow QSLs (Figures 6, 7, and 8). This indicates that magnetic reconnection along QSLs is involved in these upflows. As a particular case, some QSLs contain a separatrix inside, when the field-line mapping is discontinuous. For the case studied we find a magnetic null point at a height of about 120 Mm above the leading polarity of AR2. **This implies that** some of the computed QSLs include the separatrix (fan surface) and the spine of the null point. However, these local models can only show QSL locations relatively low in the corona (as they use a Cartesian computational box) and they are unable to tell if some of the outflows seen in the EIS maps would be able to reach the SW or not.

Therefore, we complement these local, detailed models of the AR topology with a global potential field (PFSS) magnetic topology model of magnetic nulls and separatrices, showing which magnetic field lines reach the source surface. Confirming the local LFFF and potential model results (Figure 8) we find with the PFSS model a null at a similar height (≈130 Mm) located above the leading polarity of AR2 (Figures 9 and 10) and confirm that its spine field line indeed reaches the source surface. Moreover, the spine and fan of the null point are embedded in the QSLs (computed from field line mapping reaching the photosphere or the source surface) where reconnection can occur (see Masson *et al.,* 2012). Then, at the null point and in the QSLs, interchange reconnection between closed field lines under the fan surface and open field lines, can indeed allow plasma originally confined along closed loops to gain access to open field lines and reach the solar wind. This is in agreement with the conclusions of Del Zanna *et al.* (2011).

Moreover, other thin QSLs, without separatrices, are also associated with EIS upflows. These QSLs are also expected to host magnetic reconnection; this time between closed field lines. We propose that, through reconnection of two closed asymmetric loops, the plasma-pressure gradient can drive plasma upflows (Figure 5) as was modeled by Bradshaw *et al.* (2011) for the reconnection between closed and open field lines. However, these flows will remain confined along closed loops in the solar atmosphere. Therefore, only a fraction of the upflows observed with EIS in the low corona are contributing to the SW. We have shown this in detail for AR2, which has a mixture of closed and open fields, as shown both from the PFSS model and EUV observations. The global PFSS model also shows that AR1 has no associated high-coronal null point and it is practically totally enveloped by the streamer (Figure 10), *i.e.* we do not find any significant part of AR1 in the open-field domain of CH1. Hence the upflows in AR1 observed by EIS are expected to remain confined in the low corona.

The modelling employed has its uncertainties (*e.g.* the validity of the potential and LFFF approximations may be questionable, and the chosen height of the source

surface (2.5 R_{Sun} in this case) influences the location of boundaries between open and closed field lines. Moreover, the computed magnetic field is affected by the distribution of coronal electric currents. Such effects are difficult to evaluate, and one can only rely on a comparison of the computed field lines with coronal loops. There is further uncertainty (of at most a few pixels) in overlays between EIS scans and and MDI magnetograms. However, there is no measurable difference between the QSL locations computed in the LFFF and potential field models. Moreover, the remarkable agreement between the topologies found in local and global extrapolations is quite encouraging as it indicates the robustness of the results, *e.g.* concerning the presence of the high-altitude null-point above AR2. Both the separatrix location in the global topology and the QSL location in the local LFFF extrapolation intersect the trailing positive polarity of AR at the vicinity of significant long-lived upflows. These blue-shifted upflows originate where coronal loops "separate" (e.g. Figure 3), i.e. from where, starting within a small region in the photosphere, loops (implying their field lines) connect to different regions, *i.e.* the magnetic field lines have a large connectivity gradient, which is the definition of QSLs (including separatrices). Thus, though the combined observations and modeling techniques all have their own uncertainties, the blue-shifted upflows and separating loops (traces of QSLs) are co-spatial with no uncertainty. Concerning the boundary between open and closed field lines in the global magnetic topology (Figure 9), its location is confirmed by imaging observations (*cf.* Figures 3 and 4 and the CH movie in the electronic supplement to this article). These observations clearly show that the dark CH2 intrudes AR2 when projection effects do not prevent us to look at the AR-CH boundary directly from above. So there is little doubt that the PFSS modeling captures reality in this case.

The confirmed fact that significant plasma up-flows within an AR originate at special locations in the magnetic topology, which are favourable locations for magnetic reconnection to take place, appears to contradict some previously proposed driver mechanisms of these flows, which are independent of the magnetic topology. These mechanisms are, *e.g.* impulsive heating at loop footpoints (Hara et al., 2008) and evaporation upflows due to flux emergence (Del Zanna, 2008).

We complement our coronal study with *in-situ* measurements by ACE. The large-scale coronal structures found in the PFSS model (CHs, HCS) correspond relatively well to the SW structures observed at 1 AU. From the PFSS model, we deduce that the possible outflows of both ARs should be separated by the HCS (embedded in the HPS). Indeed, within a region of slow solar wind, we found strong peaks for both the proton temperature and velocity. We associate them with the outflows from AR2 located in the close proximity to the separatrix and QSL associated with the null point and open-field lines. We also found that the higher O^{7+}/O^{6+} and C^{6+}/C^{5+} ratios in the time interval may be plausibly related to AR2, a result consistent with the observation of CH2 entering inside AR2, so in a hotter region than at the periphery of the AR. However, these ratios also indicate that the plasma associated to the velocity peak was not heated low in the corona, but at larger distances (by *e.g.* Alfvén waves or turbulence related to magnetic reconnection), since only the *in-situ* proton temperature is enhanced.

By contrast, the SW on the other side of the HPS shows only weak signatures of AR plasma. The main signature is a small increase of the O^{7+}/O^{6+} and C^{6+}/C^{5+} ratios compared to the nearby CH. This is likely to be related to the streamer overlying

AR1. Still, while the PSFF model indicates that AR1 is fully covered by closed field lines, STEREO/EUVI observations indicate the presence of some open field lines within the leading polarity. Interchange reconnection with closed fields at the periphery of AR1. This can also help to explain the characteristics of the *in-situ* plasma.

There is another remarkable difference between SW characteristics associated with the CH1–AR1 and AR2–CH2 interfaces: the former has typical FIP bias, while the latter shows a FIP bias lower than is usually found in fast SW. FIP bias involves diffusion of neutrals across field lines so it requires time to become established. There is a significant age difference between AR1 and AR2, of about one solar rotation; however this cannot explain the very low FIP bias observed, nor the lower He^{2+}–H^{+} ratio in the time interval related to AR2. Perhaps the continuous magnetic reconnection at the null-point above AR2, which is releasing plasma from closed AR loops into the solar wind, does not allow sufficient time for the FIP bias to be built up.

The most common magnetic-polarity arrangement of CH–AR complexes is that one or more ARs are flanked by two CHs of opposite magnetic polarity, with the extremes of AR polarities being the same as the CH polarities with which they interface (*e.g.* Karachik, Pevtsov, and Abramenko, 2010; Webb *et al.,* 2011). This is the magnetic configuration of the streamer belt and the configuration of the AR–CH complex under study in this article. In such a case, the interfacing open and closed field lines are of the same magnetic polarity at both sides of AR(s). We show here that in this common case magnetic interchange reconnection is possible not only at the source surface as proposed by Wang, Sheeley, and Rich (2007), but well below the source surface along null-points in pseudo-streamer configurations, which can be jointly present with the streamer. In such cases, AR plasma can gain access to open field lines and be released into the solar wind.

Sources of SW are of low radiance like CHs. The outflows from ARs, though being low-radiance regions within the AR, are much brighter than CHs, however. Can they still be sources of the SW? The plasma outflows from the periphery of AR2, which we argue to be a source of the slow SW, are places where interchange reconnection between evacuated, low-radiance, open and dense, bright, closed loops is continuously taking place, thus plasma is being released into the solar wind from the AR's rich plasma reservoir. Therefore these AR outflows must be one of the densest and therefore brightest sources of the SW.

Appendix. List of acronyms

ACE: *Advanced Composition Explorer*
AR: active region
CH: coronal hole
EIS: *EUV Imaging Spectrometer*
FIP: first ionization potential
FoV: field of view
HCS: Heliospheric Current Sheet
HPS: Heliospheric Plasma Sheet
LFFF: linear force free field
PFSS: potential field source-surface

QSL: quasi-separatrix layer
RF: rarefaction region
SIR: Stream Interaction Region
STEREO: *Solar-Terrestrial Relations Observatory*
SW: solar wind
XRT: *X-ray Telescope*

Acknowledgements

We thank the anonymous referee for constructive comments, which helped us in improving and clarifying the article. The research leading to these results has received funding from the European Commission's Seventh Framework Programme under the grant agreement No. 284461 (eHEROES project). LvDG's work was supported by the Hungarian Research grant OTKA K-081421. CHM acknowledges financial support from the Argentinean grants PICT 2007-1790, UBACyT 20020100100733 and PIP 2009-100766 (CONICET). CHM is a member of the Carrera del Investigador Científico (CONICET). PD and CHM thank ECOS-MINCyT for their cooperative science program A08U01. The work of DHB was performed under contract with the Naval Research Laboratory and was funded by the NASA Hinode program.

References

Antiochos, S.K., Mikic, Z., Titov, V.S., Lionello, R., Linker, J.A.: 2011, A model for the sources of the slow solar wind. *Astrophys. J.* **731**, 112. doi:10.1088/0004-637X/731/2/112.

Aulanier, G., Pariat, E., Démoulin, P.: 2005, Current sheet formation in quasi-separatrix layers and hyperbolic flux tubes. *Astron. Astrophys.* **444**, 961.doi:10.1051/0004-6361:20053600.

Baker, D., van Driel-Gesztelyi, L., Mandrini, C.H., Démoulin, P., Murray, M.J.: 2009, Magnetic reconnection along quasi-separatrix layers as a driver of ubiquitous active region outflows. *Astrophys. J.* **705,** 926. doi:10.1088/0004-637X/705/1/926.

Bradshaw, S. J., Aulanier, G., Del Zanna, G.: 2011, A reconnection-driven rarefaction wave model for coronal outflows. *Astrophys. J.* **743**, 66. doi:10.1088/0004-637X/743/1/66.

Brooks, D.H., Warren, H.P.: 2011, Establishing a connection between active region outflows and the solar wind: abundance measurements with EIS/Hinode. *Astrophys. J. Lett.* **727**, L13. doi:10.1088/2041-8205/727/1/L13.

Bryans, P., Young, P.R., Doschek, G.A.: 2010, Multiple component outflows in an active region observed with the EUV Imaging Spectrometer on Hinode. *Astrophys. J.* **715**, 1012. doi:10.1088/0004-637X/715/2/1012.

Culhane, J.L., Harra, L.K., James, A.M., Al-Janabi, K., Bradley, L.J., Chaudry, R.A., Rees,K., Tandy, J.A., Thomas, P., Whillock, M.C.R., Winter, B., Doschek, G.A., Korendyke, C.M., Brown, C.M., Myers, S., Mariska, J., Seely, J., Lang, J., Kent, B.J., Shaughnessy, B.M., Young, P.R., Simnett, G.M., Castelli, C.M., Mahmoud, S., Mapson-Menard, H., Probyn, B.J., Thomas, R.J., Davila, J., Dere, K., Windt, D., Shea, J., Hagood, R., Moye, R., Hara, H., Watanabe, T., Matsuzaki, K., Kosugi, T., Hansteen, V., Wikstol, Ø.: 2007, The EUV Imaging Spectrometer for Hinode. *Solar Phys.* **243**, 19. doi:10.1007/s01007- 007-0293-1.

Démoulin, P., Hénoux, J.C., Mandrini, C.H. 1994, Are magnetic null points important in solar flares ? *Astron. Astrophys*. **285**, 1023.

Démoulin, P., Hénoux, J.C., Priest, E.R., Mandrini, C.H.: 1996, Quasi-separatrix layers in solar flares. I. Method. *Astron. Astrophys*. **308**, 643.

Démoulin, P., Bagala, L.G., Mandrini, C.H., Hénoux, J.C., Rovira, M.G.: 1997, Quasi-separatrix layers in solar flares. II. Observed magnetic configurations. *Astron. Astrophys*, **325**, 305.

De Pontieu, B., McIntosh, S., Hansteen, V.H., Carlsson, M., Schrijver, C.J., Tarbell, T.D., Title, A.M., Shine, R.A., Suematsu, Y., Tsuneta, S., Katsukawa, Y., Ichimoto, K., Shimizu, T., Nagata, S.: 2007, A tale of two spicules: the impact of spicules on the magnetic chromosphere. *Publ. Astron. Soc. Japan* **59**, S655.

De Pontieu, B., McIntosh, S.W., Hansteen, V.H., Schrijver, C.J.: 2009, Observing the roots of solar coronal heating in the chromosphere. *Astrophys. J. Lett.* **701**, 1. doi:10.1088/0004-637X/701/1/L1.

Del Zanna, G.: 2003, Solar active regions: the footpoints of 1 MK loops. *Astron. Astrophys*. **406**, L5. doi:10.1051/0004-6361:20030818.

Del Zanna, G.: 2008, Flows in active region loops observed by Hinode EIS. *Astron. Astrophys*. **481**, 49. doi:10.1051/0004-6361:20079087.

Del Zanna, G., Aulanier, G., Klein, K., Török, T.: 2011, A single picture for solar coronal outflows and radio noise storms. *Astron. Astrophys.* **526**, A137. doi:10.1051/0004-6361/201015231.

Doschek, G.A., Mariska, J.T., Warren, H.P., Brown, C.M., Culhane, J.L., Hara, H., Watanabe, T., Young, P.R., Mason, H.E.: 2007, Nonthermal velocities in solar active regions observed with the Extreme-Ultraviolet Imaging Spectrometer on Hinode. *Astrophys. J. Lett*. **667**, 109. doi:10.1086/522087.

Doschek, G.A., Warren, H.P., Mariska, J.T., Muglach, K., Culhane, J.L., Hara, H., Watanabe, T.: 2008, Flows and nonthermal velocities in solar active regions observed with the EUV Imaging Spectrometer on Hinode: A tracer of active region sources of heliospheric magnetic fields? *Astrophys. J.* **686**, 1362. doi:10.1086/591724.

Elliott, H.A., McComas, D.J., Schwadron, N.A., Gosling, J.T., Skoug, R.M., Gloeckler, G., Zurbuchen, T.H.: 2005, An improved expected temperature formula for identifying interplanetary coronal mass ejections. *J. Geophys. Res*. **110**, A04103. doi:10.1029/2004JA010794.

Feldman, U., Widing, K.G.: 2003, Elemental abundances in the solar upper atmosphere derived by spectroscopic means. *Space Sci. Rev*. **107**, 665. doi:10.1023/A:1026103726147.

Foullon, C., Lavraud, B., Luhmann, J.G., Farrugia, C.J., Retino, A., Simunac, K.D., Wardle, N.C., Galvin, A.B., Kucharek, H., Owen, C.J., Popecki, M., Opitz, A., Sauvaud, J.-A.: 2011, Plasmoid releases in the heliospheric current sheet and associated coronal hole boundary layer evolution. *Astrophys. J*. **737**, 16. doi:10.1088/0004-637X/737/1/16.

Geiss, J., Gloeckler, G., von Steiger, R.: 1995, Origin of the solar wind from composition data. *Space Sci. Rev.* **72**, 49. doi:10.1007/BF00768753.

Gloeckler, G., Cain, J., Ipavich, F.M., Tums, E.O., Bedini, P., Fisk, L.A., Zurbuchen, T.H., Bochsler, P., Fischer, J., Wimmer- Schweingruber, R.F., Geiss, J., Kallenbach, R.: 1998, Investigation of the composition of solar and interstellar matter using solar wind and pickup ion measurements with SWICS and SWIMS on the ACE spacecraft. *Space Sci. Rev*. **86**, 497. doi:10.1023/A:1005036131689.

Golub, L., Deluca, E., Austin, G., Bookbinder, J., Caldwell, D., Cheimets, P., Cirtain, J., Cosmo, M., Reid, P., Sette, A., Weber, M., Sakao, T., Kano, R., Shibasaki, K., Hara, H., Tsuneta, S., Kumagai, K., Tamura, T., Shimojo, M., McCracken, J., Carpenter, J., Haight, H., Siler, R., Wright, E., Tucker, J., Rutledge, H., Barbera, M., Peres, G., Varisco, S.: 2007, The X-Ray Telescope (XRT) for the *Hinode* mission. *Solar Phys.* **243**, 63. doi:10.1007/s11207-007-0182-1.

Hara, H., Watanabe, T., Harra, L.K., Culhane, J.L., Young, P.R., Mariska, J.T., Doschek, G.A.: 2008, Coronal plasma motions near footpoints of active region loops revealed from spectroscopic observations with Hinode EIS. *Astrophys. J. Lett.* **678**, 67. doi:10.1086/588252.

Harra, L.K., Sakao, T., Mandrini, C.H., Hara, H., Imada, S., Young, P.R., van Driel-Gesztelyi, L., Baker, D.: 2008, Outflows at the edges of active regions: contribution to solar wind formation? *Astrophys. J. Lett*. **676**, 147. doi:10.1086/587485.

Harra, L.K., Archontis, V., Pedram, E., Hood, A.W., Shelton, D.L., van Driel-Gesztelyi, L.: 2012, The creation of outflowing plasma in the corona at emerging flux regions: Comparing observations and simulations, *Solar Phys*. **278**, 47. doi:10.1007/s11207-011-9855-x

Kahler, S.W., Jibben, P., DeLuca, E.E.: 2010, TRACE observations of changes in coronal hole boundaries. *Solar Phys*. **262**, 135. doi:10.1007/s11207-010-9517-4.

Karachik, N.V., Pevtsov, A.A., Abramenko, V. I.: 2010, Formation of coronal holes on the ashes of active regions. *Astrophys. J.* **714**, 1672. doi:10.1088/0004-637X/714/2/1672.

Ko, Y.-K., Raymond, J.C., Zurbuchen, T.H., Riley, P., Raines, J.M., Strachan, L.: 2006, Abundance variation at the vicinity of an active region and the coronal origin of the slow solar wind. *Astrophys. J.* **646**, 1275. doi:10.1086/505021.

Lau, Y.-T. 1993, Magnetic nulls and topology in a class of solar flare models. *Solar Phys.* **148**, 301. doi: 10.1007/BF00645092.

Lemen, J.R., Title, A.M., Akin, D.J., Boerner, P.F., Chou, C., Drake, J.F. *et al*.: 2012, The Atmospheric Imaging Assembly (AIA) on the Solar Dynamics Observatory (SDO). *Solar Phys*. **275**, 17. doi:10.1007/s11207-011-9776-8.

Liewer, P.C., Neugebauer, M., Zurbuchen, T.: 2004, Characteristics of active-region sources of solar wind near solar maximum. *Solar Phys*. **223**, 209. doi:10.1007/s11207-004-1105-z.

Luoni, M.L., Mandrini, C.H., Cristiani, G.D., Démoulin, P.: 2007, The magnetic field topology associated with two M flares, *Adv. Space Res.* **39**, 1382.

Mandrini, C.H., Démoulin, P., van Driel-Gesztelyi, L., Schmieder, B.; Cauzzi, G.; Hofmann, A.: 1996, 3D magnetic reconnection at an X-ray brigh point. *Solar Phys.* **238**, 293. doi: 10.1007/s11207-006-0205-3.

Mandrini, C.H., Démoulin, P., Schmieder, B., DeLuca, E.E., Pariat, E., Uddin, W.: 2006, Companion event and precursor of the X17 flare on 28 October 2003. *Solar Phys.* **168**, 115. doi:

Masson, S., Pariat, E., Aulanier, G., Schrijver, C.J.: 2009, The nature of flare ribbons in coronal null-point topology. *Astrophys. J.* **700,** 559. doi:10.1088/0004-637X/700/1/559.

Masson, S., Aulanier, G., Pariat, E., Klein, K.-L.: 2012, Interchange slip-running reconnection and sweeping SEP beams. *Solar Phys.* **276**, 199. doi:10.1007/s11207-011-9886-3.

Marsch, E., Wiegelmann, T., Xia, L.D.: 2004, Coronal plasma flows and magnetic fields in solar active regions. Combined observations from SOHO and NSO/Kitt Peak. *Astron. Astrophys*. **428**, 629. doi:10.1051/0004-6361:20041060.

Marsch, E., Tian, H., Sun, J., Curdt, W., Wiegelmann, T.: 2008, Plasma flows guided by strong magnetic fields in the solar corona. *Astrophys. J*. **685**, 1262. doi:10.1086/591038.

McComas, D.J., Bame, S.J., Barker, P., Feldman, W.C., Phillips, J.P., Riley, P., Griffee, J.W.: 1998, Solar wind electron proton alpha monitor (SWEPAM) for the Advanced Composition Explorer. *Space Sci. Rev*. **86**, 563. doi:10.1023/A:1005040232597.

Murray, M.J., Baker, D., van Driel-Gesztelyi, L., Sun, J.: 2010, Outflows at the edges of an active region in a coronal hole: a signature of active region expansion? *Solar Phys*. **261**, 253. doi:10.1007/s11207-009-9484-9.

Owocki, S.P., Holzer, T.E., Hundhausen, A.J.: 1983, The solar wind ionization state as a coronal temperature diagnostic. *Astrophys. J.*, **275**, 354.

Rouillard, A.P., Davies, J.A., Lavraud, B., Forsyth, R.J., Savani, N.P., Bewsher, D., Brown, D.S., Sheeley, N.R., *et al.*: 2010a, Intermittent release of transients in the slow solar wind: 1. Remote sensing observations. *J. Geophys. Res.* **115**, 4103. doi: 10.1029/2009JA014471.

Rouillard, A.P., Lavraud, B., Davies, J.A., Savani, N.P., Burlaga, L.F., Forsyth, R.J., Sauvaud, J.-A., Opitz, A., *et al.*: 2010b, Intermittent release of transients in the slow solar wind: 2. In situ evidence. *J. Geophys. Res.* **115**, 4104. doi: 10.1029/2009JA014472.

Rouillard, A.P., Sheeley, N.R., Jr., Cooper, T.J., Davies, J. A., Lavraud, B., Kilpua, E.K.J., Skoug, R.M., Steinberg, J.T.; Szabo, A., Opitz, A., Sauvaud, J.-A.: 2011, The solar origin of small interplanetary transients. *Astrophys. J.*, **734**, 7. doi: 10.1088/0004-637X/734/1/7.

Sakao, T., Kano, R., Narukage, N., Kotoku, J., Bando, T., DeLuca, E.E., Lundquist, L.L., Tsuneta, S., Harra, L.K., Katsukawa, Y., Kubo, M., Hara, H., Matsuzaki, K., Shimojo, M., Bookbinder, J.A., Golub, L., Korreck, K.E., Su, Y., Shibasaki, K., Shimizu, T., Nakatani, I.: 2007, Continuous plasma outflows from the edge of a solar active region as a possible source of solar wind. *Science* **318**, 1585. doi:10.1126/science.1147292.

Schrijver, C.J., DeRosa, M.L.: 2003, Photospheric and heliospheric magnetic fields. *Solar Phys.* **212**, 165. doi: 10.1023/A:1022908504100.

Schrijver, C.J., Title, A.M.: 2001, On the formation of polar spots in Sun-like stars. *Astrophys. J.* **551**, 1099. doi: 10.1086/320237.

Schrijver, C.J., Title, A.M., Berger, T.E., Fletcher, L., Hurlburt, N.E., Nightingale, R.W., Shine, R.A., Tarbell, T.D., Wolfson, J., Golub, L., Bookbinder, J.A., Deluca, E.E., Mc-Mullen, R.A., Warren, H.P., Kankelborg, C.C., Handy, B.N., de Pontieu, B.: 1999, A new

view of the solar outer atmosphere by the Transition Region and Coronal Explorer. *Solar Phys*. **187**, 261. doi:10.1023/A:1005194519642.

Shibata, K., Ishido, Y., Acton, L.W., Strong, K.T., Hirayama, T., Uchida, Y., McAllister, A.H., Matsumoto, R., Tsuneta, S., Shimizu, T., Hara, H., Sakurai, T., Ichimoto, K., Nishino, Y., Ogawara, Y.: 1992, Observations of X-ray jets with the YOHKOH Soft X-ray Telescope. *Publ. Astron. Soc. Japan* **44**, 173.

Smith, C.W., L'Heureux, J., Ness, N.F., Acuna, M.H., Burlaga, L.F., Scheifele, J.: 1998, The ACE magnetic fields experiment. *Space Sci. Rev*., **86**, 613. doi:10.1023/A:1005092216668.

Stenborg, G., Vourdilas, A., Howard, R.A.: 2008, A fresh view of the extreme-ultraviolet corona from the application of a new image-processing technique. *Astrophys. J.,* **674,** 1201. doi: 10.1086/525556.

Suess, S.T., Ko, Y.-K., von Steiger, R., Moore, R.L.: 2009, Quiescent current sheets in the solar wind and origins of slow wind. *J. Geophys. Res*. **114**, A04103. doi:10.1029/2008JA013704.

Tian, H., McIntosh, S.W., De Pontieu, B.: 2011, The Spectroscopic signature of quasi-periodic upflows in active region timeseries. *Astrophys. J. Lett*. **727**, L37. doi:10.1088/2041-8205/727/2/L37.

Titov, V.S., Hornig, G., Démoulin, P.: 2002, Theory of magnetic connectivity in the solar corona. *J. Geophys. Res*. **107**, 1164. doi:10.1029/2001JA000278.

Ugarte-Urra, I., Warren, H.P.: 2011, Temporal variability of active region outflows. *Astrophys. J.* **730**, 37. doi:10.1088/0004-637X/730/1/37.

von Steiger, R., Schweingruber, R. F., Wimmer, R., Geiss, J., & Gloeckler, G.: 1995, Abundance variations in the solar wind. *Adv. Space Res*. **15**, 3.

von Steiger, R., Schwadron, N.A., Fisk, L.A., Geiss, J., Gloeckler, G., Hefti, S., Wilken, B., Wimmer- Schweingruber, R.F., Zurbuchen, T.H.: 2000, Composition of quasi-stationary solar wind flows from Ulysses/Solar Wind Ion Composition Spectrometer. *J. Geophys. Res*. **105**, 27217. doi:10.1029/1999JA000358.

von Steiger, R., Zurbuchen, T.H., Geiss, J., Gloeckler, G., Fisk, L.A., Schwadron, N.A.: 2001, The 3-D heliosphere from the Ulysses and ACE solar wind ion composition experiments. *Space Sci. Rev*. **97**, 123. doi:10.1023/A:1011886414964.

Wang, Y.-M., Sheeley, N. R., Jr.: 1991, Why fast solar wind originates from slowly expanding coronal flux tubes. *Astrophys. J. Lett.* **372**, L45. doi:10.1086/186020.

Wang, Y.-M., Sheeley, N.R.J., Rich, N.B.: 2007, Coronal pseudostreamers. *Astrophys. J.* **658**, 1340. doi:10.1086/511416.

Wang, Y.-M., Ko, Y.-K., Grappin, R.: 2009, Slow solar wind from open regions with strong low-coronal heating. *Astrophys. J.* **691**, 760. doi: 10.1088/0004-637X/691/1/760.

Warren, H.P., Ugarte-Urra, I., Young, P.R., Stenborg, G.: 2011, The temperature de-pendence of solar active region outflows. *Astrophys. J.* **727**, 58. doi:10.1088/0004-637X/727/1/58.

Webb, D., Cremades, H., Sterling, A., Mandrini, C., Dasso, S., Gibson, S., Haber, D., Komm, R., Petrie, G., McIntosh, P., Welsch, B., Plunkett, S.: 2011, The global context of solar activity during the whole heliosphere interval campaign. *Solar Phys*. **274**, 57. doi:10.1007/s11207-011-9787-5

Winebarger, A.R., DeLuca, E.E., Golub, L.: 2001, Apparent flows above an active regionobserved with the transition region and coronal explorer. *Astrophys. J. Lett*. **553**, 81. doi:10.1086/320496.

Winebarger, A.R., Warren, H., van Ballegooijen, A., DeLuca, E.E., Golub, L.: 2002, Steady flows detected in extreme-ultraviolet loops. *Astrophys. J. Lett*. **567**, 89. doi:10.1086/339796.

Young, P.R., Del Zanna, G., Mason, H.E., Dere, K.P., Li, E., Lini, M., Doschek, G.A., Brown, C.M., Culhane, L., Harra, L.K., Watanabe, T., Hara, H.: 2007, EUV emission lines and diagnostics observed with Hinode/EIS. *Publ. Astron. Soc. Japan* **59**, 857.

Zhao, L., Zurbuchen, T.H., Fisk, L.A. 2009, Global distribution of the solar wind during solar cycle 23: ACE observations. *Geophys. Res. Lett*. **36**, L14104. doi: 10.1029/2009GL039181.

Zurbuchen, T.H., Fisk, L.A., Gloeckler, G., von Steiger, R.: 2002, The solar wind composition throughout the solar cycle: A continuum of dynamic states. *Geophys. Res. Lett.* **29**, 1352. doi:10.1029/2001GL013946.